University of Liège
Faculty of Applied Sciences
Department of Electrical Engineering and Computer Science

Master thesis
Model-based-design to develop sensorless fan

by Anaïs Halin

Supervised by Prof. Christophe Geuzaine and Marc Lambrechts

Master thesis submitted in partial fulfillment of the requirements for the Degree of Master of Science in Electrical Engineering

Academic year 2016-2017

Model-based-design to develop sensorless fan

Anaïs Halin,
supervised by Prof. Christophe Geuzaine and Marc Lambrechts

Electrical Engineering
University of Liège

Academic year 2016-2017

Abstract

Melexis specializes in developing robust sensorless actuators integrated circuits for automotive applications like water-oil-fuel pumps, engine cooling fans and hvac (heating, ventilating, and air conditioning) blowers.

This master thesis intends for the iterative development of a realistic electro-mechanical system model for existing hvac blowers, controlled without sensors (sensorless control loop), via electronics that measure motor current and motor voltage (self-sensing solution). It aims to predict the behavior of the fan for various control algorithms. Purpose is to accelerate future designs with efficient and robust control algorithms for self-sensing fans and pumps.

In order to reach these objectives, the first step is to select the modelling tool, then to create a model (first in open-loop, then in closed-loop) with available BLDC (brushless direct current) motor systems knowhow from Melexis application engineers. This is done by performing iterative fitting with real system behaviour and simplifying the model to the essence.

Furthermore, this document presents a way to find the electrical and mechanical motor's parameters which are necessary to run the model. Finally, the model allowed to perform a parametric analysis for hvac blowers enabling to better understand the key parameters influencing the behavior of such systems.

Figure 1: hvac blower fan used in the air conditioning system of a car.

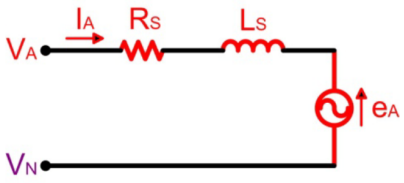

Figure 2: Equivalent circuit of a BLDC motor for one of its phases. The following assumptions are considered: the motor is not saturated; stator resistances of all the windings are equal (R_S), self inductances are constant (L_S) and mutual inductances (M) are zero; iron losses are negligible.

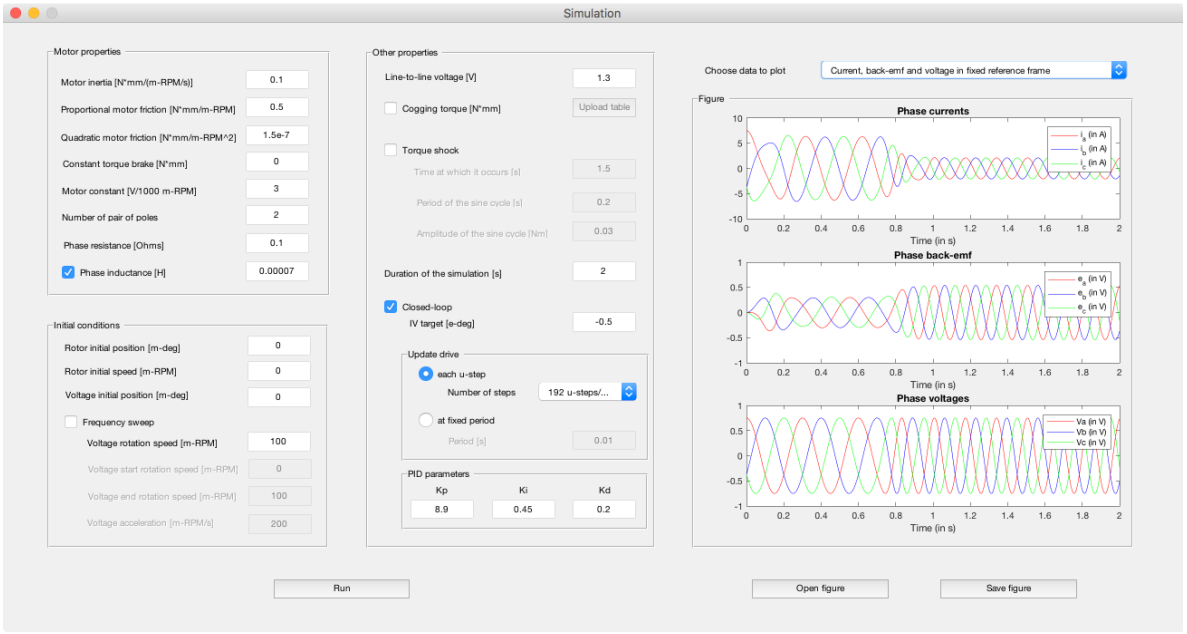

Figure 3: Window of the Graphical User Interface (GUI). On the left part of the window are the parameters of the simulation and the pushbutton to run the model. On the other side, the results are displayed and the data to plot can be chosen via a popup menu.

Acknowledgements

I would like to thank everyone who supported me throughout this master thesis, I am thankful for the time you all have dedicated to me.

I would especially like to express my gratitude to my supervisors Professor Christophe Geuzaine and Marc Lambrechts.

I also thank Melexis for having welcomed me.

Finally, I would like to thank all the Professors of the Faculty of Applied Sciences, and especially the Professors who agreed to be part of my jury.

Anaïs Halin

Contents

List of Abbreviations

BEMF back electromotive force.

BLDC brushless direct current.

DC direct current.

EMF electromotive force.

GUI graphical user interface.

HVAC heating, ventilating, and air conditioning.

IC integrated circuit.

PM permanent magnet.

PMSM permanent magnet DC synchronous motor.

RMS root mean square.

RPM revolutions per minute.

List of Symbols

$\mathbf{E}$	back-emf.
$\boldsymbol{e_a}, \boldsymbol{e_b}, \boldsymbol{e_c}$	phase back-emf.
$\mathbf{I}$	current.
$\boldsymbol{i_a}, \boldsymbol{i_b}, \boldsymbol{i_c}$	phase currents.
$\boldsymbol{i_\alpha}, \boldsymbol{i_\beta}$	alpha and beta currents.
$\boldsymbol{i_d}, \boldsymbol{i_q}$	direct and quadrature currents.
$\mathbf{J}$	inertia.
$\boldsymbol{K}_e$	motor constant (translation rotation speed to back-emf).
$\boldsymbol{K}_T$	motor constant (translation current to torque).
$\mathbf{L}$	self-inductance.
$\boldsymbol{\Omega}$	rotor acceleration.
$\boldsymbol{\omega}$	rotor angular speed.
$\mathbf{p}$	number of pole pairs.
$\mathbf{R}$	resistance.
$\mathbf{t}$	time.
$\boldsymbol{\theta}_e$	electrical rotor angle.

$\boldsymbol{\theta}_m$	mechanical rotor angle.
$\boldsymbol{T}_e$	electromagnetic torque.
$\boldsymbol{T}_f$	friction torque.
$\boldsymbol{T}_l$	load torque.
$\mathbf{V}$	DC voltage.
$\boldsymbol{v_a}, \boldsymbol{v_b}, \boldsymbol{v_c}$	phase voltages.

Chapter 1

Introduction

This master thesis was linked to an internship within the Belgian Micro-Electronic Integrated Systems Company, Melexis N.V. Melexis, as its name suggests, is a global supplier of micro-electronic semiconductor solutions. Among a wide range of product, the Company specializes in developing robust sensorless actuators IC's for automotive applications like water-oil-fuel pumps, engine cooling fans and hvac blowers. The application engineers of the Business Unit Actuators develop new products and find solutions for the customer needs. They work in a very pratical way. Their ultimate goal is to make a product work.

The aim of this master thesis is to develop a realistic electro-mechanical system model that can predict the behavior of hvac blowers. The model can thus be used as a modelling tool to answer "what if" questions or explain theoriticaly some behaviors. The second objective is to investigate how to identify the model electrical and mechanical parameters. Finally, a parametric analysis shows the influence of electrical and mechanical parameters on motor systems. Purpose of the thesis is to start model-based-design for motor control in Melexis:

- starting from Matlab-Simulink simulations for sensorless BLDC control
- generating software routines from this control model to include in Melexis' embedded motor control IC's

in order to accelerate future designs with efficient and robust control algorithms for self-sensing fans and pumps. Currently, they prototype the application directly on the chip,

using user-intensive embedded software development and iterations of trial - testing - correcting.

In order to reach these objectives, the first step is to select the modelling tool. This master thesis has been entirely performed using Matlab. The second step is to derive and implement a mathematical model in open-loop and in closed-loop. This will be done by performing iterative fitting with real system behaviour and simplifying the model to the essence. Despite the name, BLDC motors are actually a type of permanent magnet synchronous motors (PMSM).

High efficiency and low noise are key requirements for fan systems. A control strategy based on motor current and voltage measurements (IV measurements) can be applied which leads to high efficiency. The brushless 3-phase motors are controlled without sensors, via electronics that measure motor current and motor voltage (self-sensing solution). Sinusoidal phase currents, in turn, contribute to smooth torque, and hence, low noise.

1.1 Overview

Firstly a literature study in the relevant areas was performed. Chapter 2 describes the background. A model of BLDC motors is first achieved in open-loop in Chapter 3. Then a closed-loop model is implemented following different scenarios and algorithms in Chapter 4. The GUI (Graphical User Interface) is presented in Chapter 5, in which results of the simulation are also given and analyzed. Open-loop electrical and mechanical systems are characterized in Chapter 6 and Chapter 7. These chapters allow to identify the model parameters. Electrical and mechanical parametric analysis are performed in Chapter 8 and Chapter 9, giving the impact of parameters on the behavior of the system. Conclusions are drawn in Chapter 10 along with future work recommendations. Finally, Appendix A is a non-technical chapter dedicated to the strategy aspects of Melexis.

Chapter 2

Background

The following chapter is theoretical about BLDC motors and its mathematical modelling. It also presents the reference frames used in this work, and finally defines the cogging torque.

2.1 BLDC motors

The brushless DC motor (BLDC) is a synchronous electric motor which, from a modelling perspective, looks like a DC motor. It exhibits a linear relationship on the one hand between current and torque, and on the other hand between back-emf and rotation speed. It is an electronically controlled commutation system, while brushed motors have a mechanical commutation. Additionally, the electromagnets do not move, and the permanent magnets rotate. A diagram of the BLDC motor is shown, on Figure 2.1.

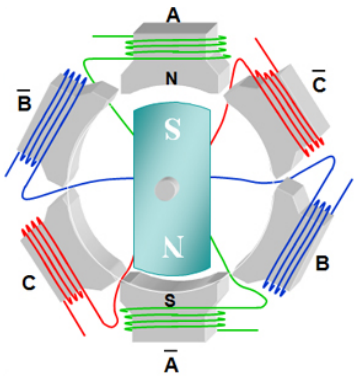

Figure 2.1: BLDC motor cross section. Source: [15].

It is constructed with a permanent magnet rotor and a stator made out of laminated steel stacked up to carry windings. Electrical energy is converted to mechanical energy by the magnetic attractive forces between the permanent magnet rotor and a rotating magnetic field induced in the stator [4]. Therefore, motor operation is based on the attraction or repulsion between magnetic poles.

BLDC motors have many advantages over brushed DC motors and induction motors. Better speed versus torque characteristics, high dynamic response, high efficiency and reliability, long operating life, and noiseless operation are some of their pros.

There are two types of permanent magnet brushless DC motors which depend on their back-emf waveforms. One has a stator winding which is trapezoidally wound to produce a trapezoidal (six-step) back-emf (back-electromotive force) waveform. The other one has a sinusoidally distributed winding with sinusoidal back-emf. Sometimes, the first one is referred to as BLDC motor while the second is called PMSM (Permanent Magnet Synchronous Motor). Star wound motors with sinusoidal waveforms are considered hereafter but BLDC motors and PMSM's will be used interchangeably to refer to this kind of motors.

The control of BLDC motors can be done in sensor or sensorless mode. The advantage of sensorless BLDC motor control is that the sensing part can be omitted, and thus overall costs and size can be reduced. However, the disadvantages of sensorless control are the higher requirements for control algorithms and more complicated electronics [5].

In order to obtain a noiseless operation, a constant torque is desired. The torque of the BLDC motor is mainly influenced by the waveform of back-emf (the voltage induced into the stator winding due to rotor movement) and a sinusoidal motor produces smoother electromagnetic torque than a trapezoidal motor. Moreover it can be shown that even if there is a phase shift between voltage and back-emf, the torque is a constant in steady-state.

A three-phase inverter is used to drive the three-phase BLDC motor as illustrated on Figure 2.2. It is indeed electrically commutated by power switches instead of brushes. The easiest way to commutate a BLDC motor is the trapezoidal commutation. The generated torque has a considerable torque ripple which occurs at each step of the

trapezoidal (or six-step) commutation. The six-step commutation typically energizes two motor phase windings at any commutation sequence. It uses 6 distinct steps (i.e. 6 positions per 360 electrical degrees), each according to an angle of 60° electrical turning angle. The control is based on position feedback. According to the position of the rotor, the inverter is in one of its 6 states. The main advantage of the trapezoidal commutation scheme is its simplicity. The downside is a torque ripple, especially at low speeds.

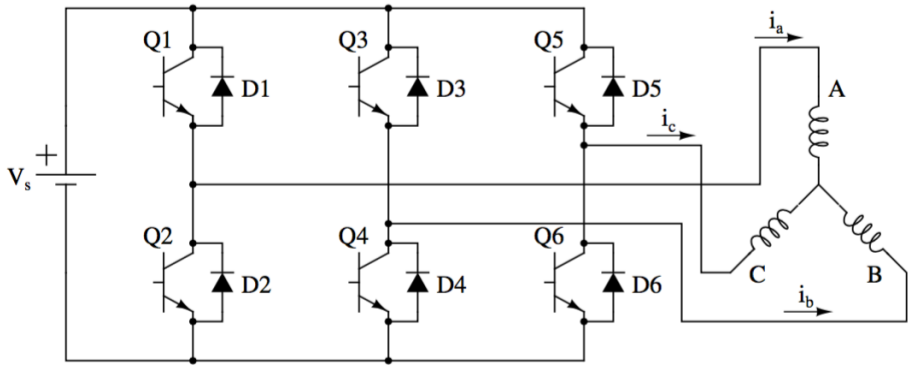

Figure 2.2: BLDC motor drive circuit, composed of the three-phase bldc motor and an inverter circuit (three-phase full-bridge structure). Source: [1].

An alternative to the simple trapezoidal commutation is to energize all three phases with sinusoidal currents. That means that the flat peaks that show up in the current waveform with trapezoidal commutation are replaced by sinusoidally shaped waveforms. In addition, all three phases are continuously energized, while with trapezoidal commutation, one phase is always off. That gives much smoother torque generation and enables more precise control. However, to generate a current waveform which is close to sinusoidal, a continuous position calculation is necessary. A finer resolution than the 60° which suffices for trapezoidal commutation is needed. Indeed, a resolution in the range of one degree is reasonable but the finer the resolution, the more precise the control [7].

2.2 Mathematical model

The model of the armature winding for the BLDC motor is expressed as follows [13]:

$$v_a = Ri_a + L\frac{di_a}{dt} + e_a \tag{2.1}$$

$$v_b = Ri_b + L\frac{di_b}{dt} + e_b \tag{2.2}$$

$$v_c = Ri_c + L\frac{di_c}{dt} + e_c \tag{2.3}$$

where L is armature self-inductance $[H]$,
R - armature resistance $[\Omega]$,
v_a, v_b, v_c - terminal phase voltage $[V]$,
i_a, i_b, i_c - motor input current $[A]$,
and e_a, e_b, e_c - motor back-emf [V].

The equivalent circuit for one phase is represented on Figure 2.3.

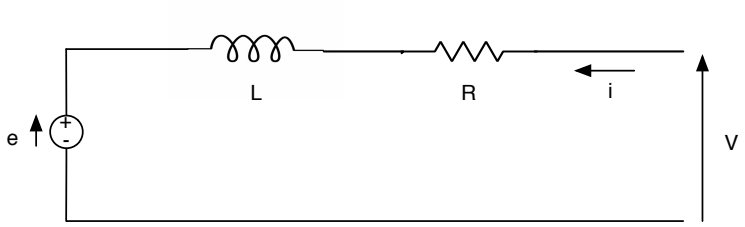

Figure 2.3: Equivalent circuit of the BLDC motor for one phase.

In the 3-phase BLDC motor, the back-emf is related to a function of rotor position and the back-emf of each phase has 120 degrees phase angle difference so that the equation of each phase should be as follows:

$$e_a = K_e f(\theta_e)\omega \tag{2.4}$$

$$e_b = K_e f(\theta_e - 120)\omega \tag{2.5}$$

$$e_c = K_e f(\theta_e + 120)\omega \tag{2.6}$$

where K_e is back-emf constant $[V/m - RPM]$[1],
θ_e - electrical rotor angle $[e - degrees]$,
ω - rotor speed $[m - RPM]$.

The electrical rotor angle is equal to the mechanical rotor angle multiplied by the number of pole pairs p:

$$\theta_e = p\theta_m \tag{2.7}$$

where θ_m is mechanical rotor angle $[m - degrees]$.

The total torque output can be represented as a summation of that of each phase. Next equation represents the total torque output, or electromagnetic torque:

$$T_e = \frac{e_a i_a + e_b i_b + e_c i_c}{\omega} = K_T \frac{3}{2} i_q \tag{2.8}$$

where T_e is total torque output $[Nm]$,
K_T - motor constant $[Nm/A]$,
i_q - quadrature current $[A]$.

The equation of the mechanical part is represented as follows:

$$T_e - T_l = J\frac{d\omega}{dt} + T_f \tag{2.9}$$

where T_l is load torque $[Nm]$,
J - inertia of rotor and coupled shaft $[kgm^2]$,
T_f - friction torque $[Nm]$.

[1]The back-emf constant is expressed in volts per mechanical RPM (revolutions per minute). The $m-$ and $e-$ symbols before a unit respectively means mechanical and electrical referring to mechanical and electrical angles which are linked by the number of pole pairs as in (2.7).

2.3 Reference frames

Different reference frames are used in the modelling in order to simplify some electromagnetic equations and express phase currents, direct and quadrature currents in the most consistent way. Three reference frames, illustrated on Figure 2.4, are defined :

- a three-phase reference frame (a,b,c),
- a two-phase reference frame (α,β),
- a rotating reference frame (d,q).

The α,β frame is fixed to the stator, while the d,q frame is fixed to the rotor.

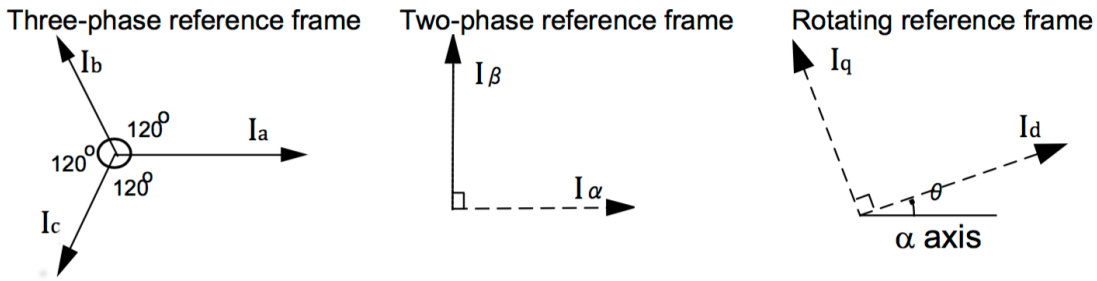

Figure 2.4: Different reference frames. Source: [12].

The three-phase currents i_a, i_b and i_c are in the fixed three-phase reference frame, composed of the three axes A, B and C at an angle of 120 degrees to each other. The Clarke transform uses the three-phase currents i_a, i_b and i_c to calculate currents in the two-phase orthogonal stator axis: i_α and i_β. These two currents in the fixed coordinate stator phase are transformed to the i_d and i_q currents components in the d,q frame with the Park transform.

The i_α (along α-axis) and i_β (along β-axis) currents are perpendicular to each other and expressed in the orthogonal stationary reference frame. They can be obtained from the phase-currents in the following way:

$$i_\alpha = \frac{2}{3} \cdot (i_a - \frac{1}{2} i_b - \frac{1}{2} i_c) \tag{2.10}$$

$$i_\beta = \frac{2}{3} \cdot (\frac{\sqrt{3}}{2} i_b - \frac{\sqrt{3}}{2} i_c) \tag{2.11}$$

or in a matrix representation

$$\begin{bmatrix} i_\alpha(t) \\ i_\beta(t) \end{bmatrix} = \frac{2}{3} \begin{bmatrix} 1 & -\frac{1}{2} & -\frac{1}{2} \\ 0 & \frac{\sqrt{3}}{2} & -\frac{\sqrt{3}}{2} \end{bmatrix} \begin{bmatrix} i_a(t) \\ i_b(t) \\ i_c(t) \end{bmatrix} \tag{2.12}$$

The Clarke's transformation (also known as the alpha-beta transformation), defined in (2.12), preserves the amplitude of the electrical variables it is applied to. Indeed, considering a three-phase symmetric, direct, current sequence

$$\begin{aligned} i_a(t) &= \sqrt{2} I \cos(\theta(t)) \\ i_b(t) &= \sqrt{2} I \cos(\theta(t) - 120) \\ i_c(t) &= \sqrt{2} I \cos(\theta(t) + 120) \end{aligned}$$

where I is the rms of i_a, i_b, i_c, to which the transformation is applied, it results in

$$\begin{aligned} i_\alpha(t) &= \sqrt{2} I \cos(\theta(t)) \\ i_\beta(t) &= \sqrt{2} I \sin(\theta(t)) \end{aligned}$$

Direct and quadrature currents, i_d and i_q, use a frame of reference on the rotor. As illustrated on Figure 2.4, i_q is 90 degrees further than i_d and they rotate at the speed of the rotor so that i_d has an angle equal to the rotor angle θ with the α-axis. The i_d and i_q currents can be computed as follows:

$$\begin{aligned} i_d &= i_\alpha \cos(\theta) + i_\beta \sin(\theta) \\ i_q &= i_\beta \cos(\theta) - i_\alpha \sin(\theta) \end{aligned}$$

or in a matrix representation

$$\begin{bmatrix} i_d \\ i_q \end{bmatrix} = \begin{bmatrix} \cos(\theta) & \sin(\theta) \\ -\sin(\theta) & \cos(\theta) \end{bmatrix} \begin{bmatrix} i_\alpha \\ i_\beta \end{bmatrix} \tag{2.13}$$

The direct and quadrature currents, i_d and i_q, can also be expressed in terms of the phase currents i_a, i_b and i_c, defining the Park's transformation:

$$\begin{bmatrix} i_d \\ i_q \end{bmatrix} = \frac{2}{3} \begin{bmatrix} \cos(\theta) & \cos(\theta - 120) & \cos(\theta + 120) \\ -\sin(\theta) & -\sin(\theta - 120) & -\sin(\theta + 120) \end{bmatrix} \begin{bmatrix} i_a(t) \\ i_b(t) \\ i_c(t) \end{bmatrix} \tag{2.14}$$

The amplitude of the current (or peak current) can be obtained as follows :

$$\begin{aligned} I &= \sqrt{i_d^2 + i_q^2} \\ &= \sqrt{i_\alpha^2 + i_\beta^2} \end{aligned}$$

2.4 Cogging torque

The cogging torque of electrical motors is the torque due to the interaction between the permanent magnets of the rotor and the stator slots. The construction of a slotted motor is shown on Figure 2.5.

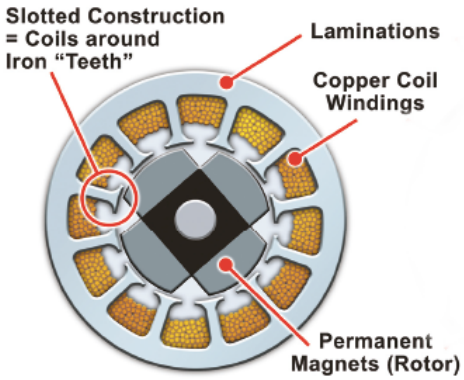

Figure 2.5: Construction of a slotted motor. Source: [3].

This torque is position dependent and its periodicity per revolution depends on the number of magnetic poles and the number of teeth on the stator as illustrated on Figure 2.6.

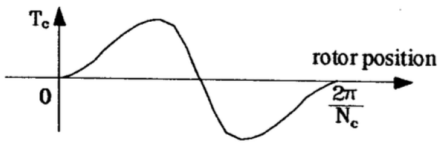

Figure 2.6: Typical cogging torque waveform. T_c is the cogging torque and N_c is the period per revolution. Source: [16].

It manifests itself by the tendency of a rotor to align in a number of stable positions even when the machine is unexcited. The cogging torque is an undesirable effect that prevents the smooth rotation of the rotor and results in noise. It is especially prominent at lower speeds. It results in torque as well as speed ripples. At high speed, the motor moment of inertia filters out the effect of cogging torque[2].

As illustrated on Figure 2.7, each tooth of the stator is strongly attracted to each passing PM pole. There are two positions of the rotor pole which will result in a zero cogging torque. The first one is when the PM pole is centered on a stator tooth. This is a stable point: if the rotor is moved from this position, a restoring torque will occur and the magnet will attempt to reestablish this position. The second one is centered at the transition between two teeth. This is an unstable point: if the rotor is moved from this position, a non-restoring torque will develop and the magnet will seek to depart from this position and be attracted by the nearest tooth center [6].

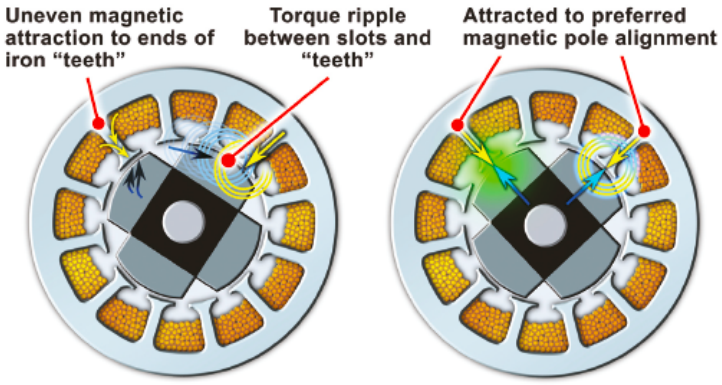

Figure 2.7: Cogging effect in a slotted motor. Source: [3].

[2]The mechanical part of the motor can be represented as a low-pass filter where the inertia is a capacitor and the friction a resistance, which explains why the high frequency components of a torque are filtered out.

Chapter 3

Open-loop modelling

This chapter deals with the open-loop modelling of BLDC motors. The model is implemented on Matlab using *ode45*.

The model is focusing on hvac blowers with the following assumptions:

- sinusoidal back-emf,
- balanced system where all three phases have equal impedance values: $i_a(t) + i_b(t) + i_c(t) = 0$, $R_a = R_b = R_c$ and $L_a = L_b = L_c$
- friction/load of the type: $T = a * \omega^2 + b * \omega + c$, where a, b and c are constants.

The model is built step by step. For this purpose, it is divided into three consistent parts: the electrical, the mechanical and the electro-mechanical parts.

3.1 Electrical part

The main purpose here is to estimate the shape and the amplitude of the back-emf. It is given for each phase by (2.4), (2.5) and (2.6), where $f(\theta_e)$ is a sinusoidal function (according to the assumptions), which leads to

$$e_a = K_e\,\omega\cos(\theta_e + 90) \tag{3.1}$$

$$e_b = K_e\,\omega\cos(\theta_e + 90 - 120) \tag{3.2}$$

$$e_c = K_e\,\omega\cos(\theta_e + 90 + 120) \tag{3.3}$$

or equivalently

$$e_a = -K_e\,\omega\sin(\theta_e) \tag{3.4}$$

$$e_b = -K_e\,\omega\sin(\theta_e - 120) \tag{3.5}$$

$$e_c = -K_e\,\omega\sin(\theta_e + 120) \tag{3.6}$$

where $(\theta_e + 90)$ means that the back-emf is always 90 degrees further than the rotor. Indeed, according to Faraday's law[1], the back-emf is phase shifted by 90 degrees compared to the flux.

3.2 Mechanical part

The mechanical part consists in computing the mechanical torque T_{mech}. Firstly, this torque is defined as the frictional torque $T_{friction}$. Then, the cogging torque T_{cog} and a torque shock T_{shock} can optionally be added to the model so that the mechanical torque is given by

$$T_{mech} = T_{friction} + T_{cog} + T_{shock} \tag{3.7}$$

According to the assumptions, there is a relation between the frictional torque $T_{friction}$ and the rotational speed ω. Three terms are considered: a constant, a proportional and a quadratic term. Therefore, the following equation is used:

$$T_{friction} = Fr2_m * \omega^2 + Fr_m * \omega + T_0 \tag{3.8}$$

where
$Fr2_m$ is the friction of the motor system, modeled quadratic to speed,
Fr_m - friction of the motor system, modeled proportional to speed,
T_0 - constant torque brake.

The modelling of the cogging torque is not the concern of this work. A table of the cogging torque as a function of the mechanical position of the rotor, $T_{cog}(\theta_m)$, over one revolution of 360 degrees need to be uploaded. Then a spline interpolation is performed

[1]Faraday's law is given by $V = -N\frac{d\phi}{dt}$, where V is the induced voltage, ϕ the magnetic flux and N the number of turns.

in order to get the value of the cogging torque at each desired rotor position. This way, we are able to take the cogging torque into account in our model.

The torque shock as illustrated on Figure 3.1 consists of one sine cycle of defined period and amplitude, which occurs at a defined time t.

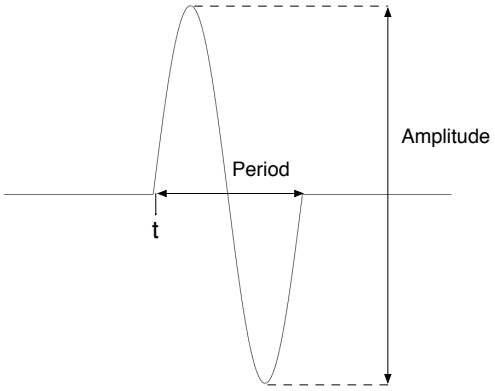

Figure 3.1: Parameters of a torque shock.

3.3 Electro-mechanical part

The driving torque (also called total torque output or electromagnetic torque) can be computed using (2.8). However, using this formula in the modelling can cause problems when the rotation speed ω is equal to zero. Therefore, it is simplified using (2.4), (2.5) and (2.6) which leads to

$$T_{drive} = \frac{K_e}{1000} \cdot \frac{60}{2\pi} \cdot (\cos(\theta_e + 90)i_a + \cos(\theta_e + 90 - 120)i_b + \cos(\theta_e + 90 + 120)i_c) \quad (3.9)$$

where the factor $\frac{60}{1000 \cdot 2\pi}$ appears to keep consistent units[2] .

[2]In (2.8) ω is expressed in rad/s while in (2.4), (2.5) and (2.6), ω is in $m - RPM$, and K_e is in $V/1000m - RPM$.

As K_T and K_e are related, the driving torque can be expressed in terms of the constant K_T and the quadrature current i_q using (2.14):

$$T_{drive} = K_T \cdot (\cos(\theta_e + 90)i_a + \cos(\theta_e + 90 - 120)i_b + \cos(\theta_e + 90 + 120)i_c) \quad (3.10)$$

$$= K_T \cdot \frac{3}{2} \cdot i_q \quad (3.11)$$

Indeed, according to their respective units:

$$K_e[V/(1000 \cdot m - RPM)] \cdot \frac{60}{2\pi} = K_T[Nmm/A] \quad (3.12)$$

or

$$K_e[V/(m - rad/s)] = K_T[Nm/A] \quad (3.13)$$

3.4 Open-loop model

The electrical part, mechanical part and electro-mechanical part are then combined in order to obtain the final open-loop model.

We first compute the acceleration torque as follows:

$$T_{accel} = T_{drive} - T_{mech} \quad (3.14)$$

Then, *ode45*[3] can be used to compute the rotor rotation speed

$$\frac{d\omega}{dt} = \frac{T_{accel}}{J}, \quad (3.15)$$

the rotor position

$$\frac{d\theta}{dt} = \omega, \quad (3.16)$$

the voltage rotation speed

$$\frac{dV_{speed}}{dt} = \begin{cases} V_{accel} & \text{if frequency sweep} \\ 0 & \text{otherwise} \end{cases}, \quad (3.17)$$

[3] *Ode45* is a differential equations solver defined in Matlab.

the voltage position

$$\frac{dV_{pos}}{dt} = V_{speed}, \tag{3.18}$$

and finally, the phase currents

$$\frac{di_a}{dt} = \frac{v_a - R_a i_a - e_a}{L}, \tag{3.19}$$

$$\frac{di_b}{dt} = \frac{v_b - R_b i_b - e_b}{L}, \tag{3.20}$$

$$\frac{di_c}{dt} = \frac{v_c - R_c i_c - e_c}{L}. \tag{3.21}$$

If the inductance is neglected in the simulation, the phase currents are simply computed as:

$$i_a = \frac{v_a - e_a}{R_a} \tag{3.22}$$

$$i_b = \frac{v_b - e_b}{R_b} \tag{3.23}$$

$$i_c = \frac{v_c - e_c}{R_c} \tag{3.24}$$

Chapter 4

Closed-loop modelling

This chapter deals with the closed-loop implementation of the system. A PID controller is used for the regulation.

4.1 PID controller

A PID controller (Figure 4.1) continuously computes an error value e(t) as the difference between a desired setpoint r(t) and a measured process variable y(t) and applies a correction based on proportional, integral, and derivative terms (denoted P, I, and D respectively). The controller attempts to minimize the error over time by adjustment of a control variable u(t) to a new value determined by a weighted sum:

$$u(t) = K_p\, e(t) + K_i \int_0^t e(\tau)d\tau + K_d\, \frac{de(t)}{dt} \tag{4.1}$$

where K_p, K_i, K_d denote the coefficients for the proportional, integral, and derivative terms. However, the model referred to in this work implements a discrete PID controller which means that approximate discrete time integrals and derivatives are used.

The algorithm of control which has been implemented consists in measuring the IV angle, i.e. angle between the current and the voltage, and updating the drive (rotation speed) a fixed amount of times during one electrical rotation of the voltage. Thereby, if the drive is updated x times during one electrical rotation of the voltage, one says that the update occurs every x u-steps/360 electrical.

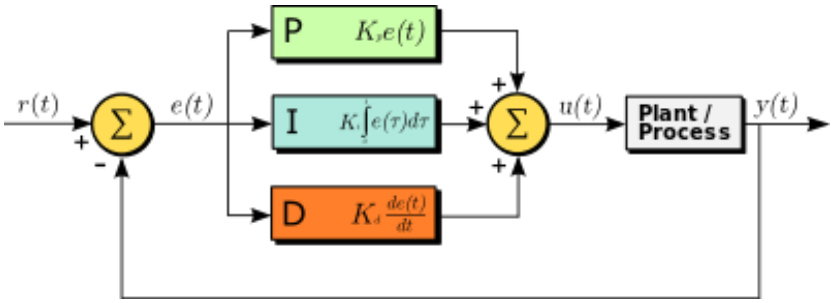

Figure 4.1: A block diagram of a PID controller in a feedback loop. r(t) is the desired process value ("set point" or "target"), and y(t) is the measured process value. Source: [14].

Three scenarios are studied:

- u-step scenario 1: 192 u-steps/360 electrical,
- u-step scenario 2: 48 u-steps/360 electrical,
- u-step scenario 3: 6 u-steps/360 electrical.

It is also possible to update the drive at fixed periods of time. The desired period can be entered in the GUI - the GUI is shown on Figure 4.2.

Therefore, in this case, the error signal e(t) is the IV error defined as the difference between the IV target and the IV measured at the time t, and u(t) is the rotation speed of the voltage. If the IV error is positive, the rotation speed must be increased while if the IV error is negative, the speed must be decreased. Indeed, if a zero IV target is considered, a positive IV error is obtained with a negative IV measured. However, a negative IV measured means that the current lags behind the voltage, which also means that the back-emf leads the voltage. Therefore, the rotation speed of the voltage must be increased. The pseudocode which implements the discrete PID algorithm is given page 19.

Initialization:

previous_integral = V_{speed}

previous_error = target - measured_value

Regulation:

error = target - measured_value

proportional = K_p * error

integral = previous_integral + K_i * error

derivative = K_d * (previous_error - error)

output = proportional + integral + derivative

previous_integral = integral

previous_error = error

The closed-loop is activated once the system has reached steady-state. Therefore, during start-up time, the system is in open-loop. Two variables are initialized before the regulation begins. The current error is obtained by subtracting the measured_value (IV angle) from the target. Then, proportional, integral and derivative values are computed using three preset gain terms (the proportional gain, the integral gain and the derivative gain entered in the GUI by the user). These are then combined to derive the output value, u(t), which will be defined as the new rotation speed of the voltage, V_{speed}. The current error as well as the integral value are stored for the next iteration. At the next u-step or after the period chosen by the user in the GUI, the regulation step runs again.

In practice, *ode45* is paused at each u-step or each time period depending on the algorithm to execute the initialization or regulation. Then, *ode45* is re-started taking into account the output of the PID, i.e. the new V_{speed}.

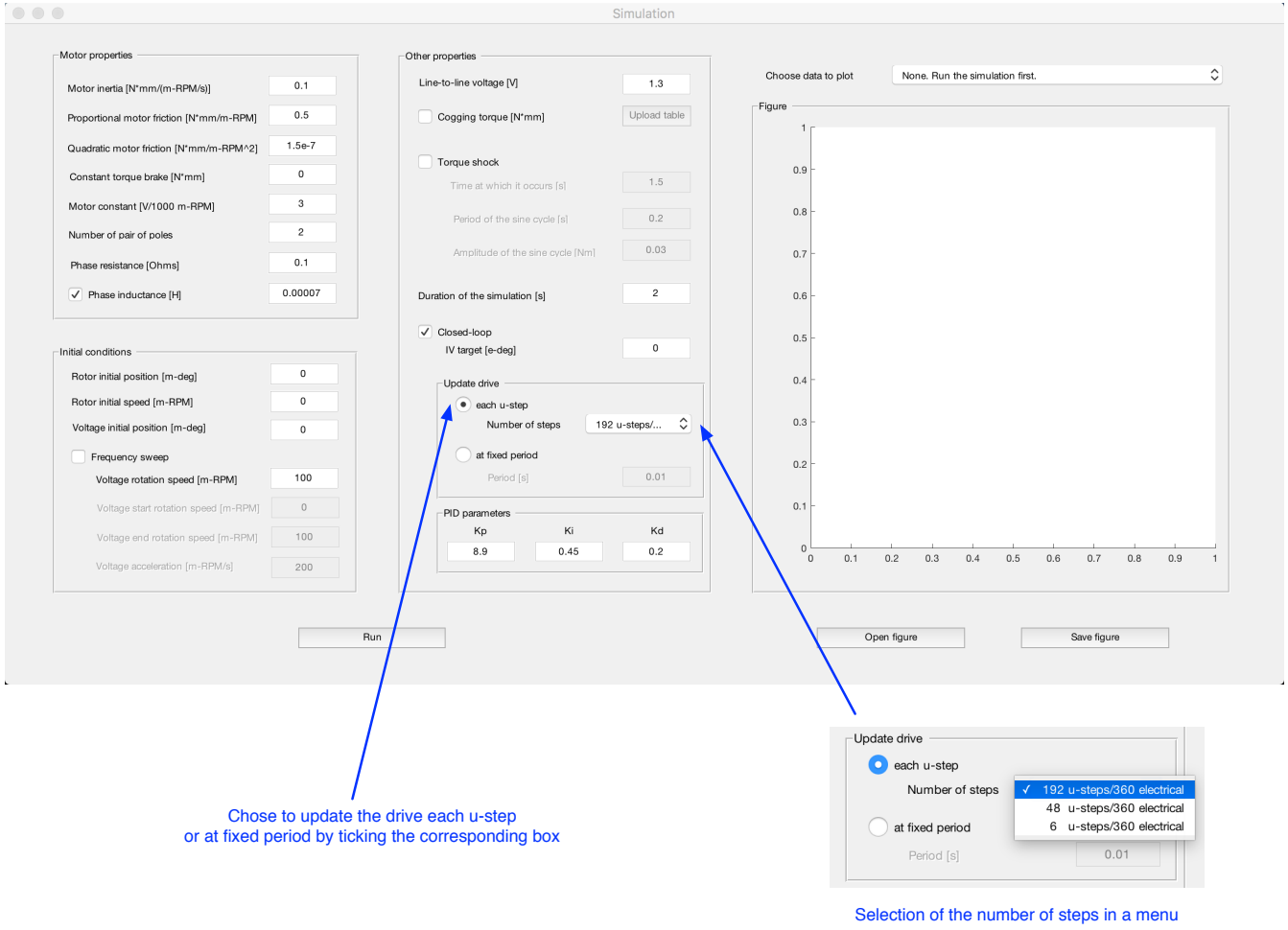

Figure 4.2: Graphical User Interface. To run the model in closed-loop, the closed-loop box must be ticked. It is then possible to choose the desired scenario for the closed-loop. The number of steps can be selected in a menu and the period can be entered via an editable box. Likewise, the IV target as well as the PID parameters can be chosen via editable boxes.

4.2 PID parameters

Concerning the tuning of the controller, manual tuning seems to be the best approach thanks to its simplicity. Indeed, it is difficult to apply a method such as Ziegler-Nichols since the motor is a quite complex system. The basic rules of manual controller tuning are summarized in Table 4.1 which shows the different effects of increasing a parameter. From this table, one sees that if the controller is slower than required, a smaller proportional gain is desirable for example. In order to find the optimal values of the K_p, K_i and K_d gains, manual tuning is done by setting the integral gain to its maximum value and the derivative term to zero and increasing the proportional gain until the loop oscillates at a constant amplitude. Then set the proportional gain to half of that value and adjust the integral gain so it corrects for any offset within an acceptable period. Finally, increase the derivative gain until overshoot is minimized.

Parameter	Rise time	Overshoot	Steady-state error	Stability
K_p	Decrease	Increase	Decrease	Degrade
K_i	Decrease	Increase	Eliminate	Degrade
K_d	Minor change	Decrease	No effect in theory	Improve if K_d small

Table 4.1: Manual tuning - Effects of increasing a parameter independently.

The PID parameters can be entered by the user in the GUI via editable boxes (cf. Figure 4.2).

4.3 Selection of the target

The IV target can also be entered by the user in the GUI (cf. Figure 4.2), and should be chosen so that the motor is driven efficiently. For this purpose, the direct current i_d should be zero. This is obtained if the current and the back-emf are aligned (IB_angle $= 0$). Insofar as the inductance can be neglected ($L = 0$), when current and back-emf are aligned, the voltage is also aligned with the current, which means that the IV target should be zero for an efficient drive. When the inductance is taken into account however, the IV target should be slighty different from zero. Indeed, in this case, when the IB angle and thus the direct current are equal to zero, the IV angle is not equal to zero anymore.

4.4 Influence of the number of steps

One notices on Figure 4.3 that the controller is very slow when updating the drive every 6 u-steps/360 electrical. In fact, in this case, the IV angle decreases a lot before finally converging to zero. This occurs since first the back-emf increases and then the alignement occurs. Theferore, the torque increases slowly. In the case of 48 and 192 u-steps/360 electrical, keeping the PID parameters constant, the controller is much quicker as illustrated on Figure 4.4 and Figure 4.5. The alignment occurs sooner and therefore, the IV angle decrease is smaller. Furthermore, for the same PID parameters, the overshoot increases as the number of u-steps gets bigger. In order to avoid this kind of problems, the PID parameters must be properly chosen depending on the number of steps.

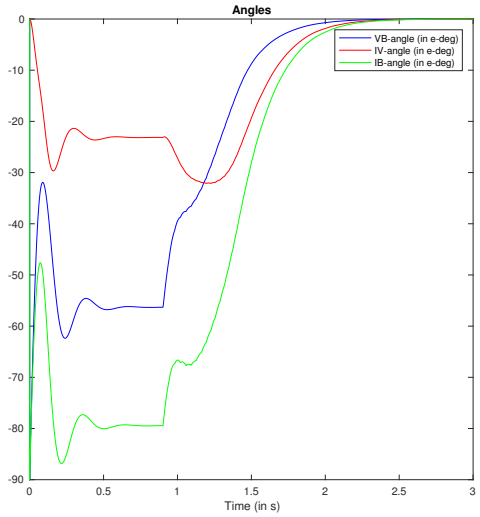

Figure 4.3: $K_p = 10,\ K_i = 1.4,\ K_d = 2$ and 6 u-steps/360 electrical

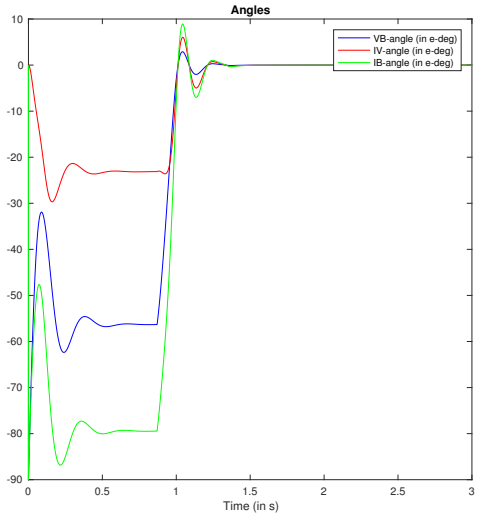

Figure 4.4: $K_p = 10,\ K_i = 1.4,\ K_d = 2$ and 48 u-steps/360 electrical

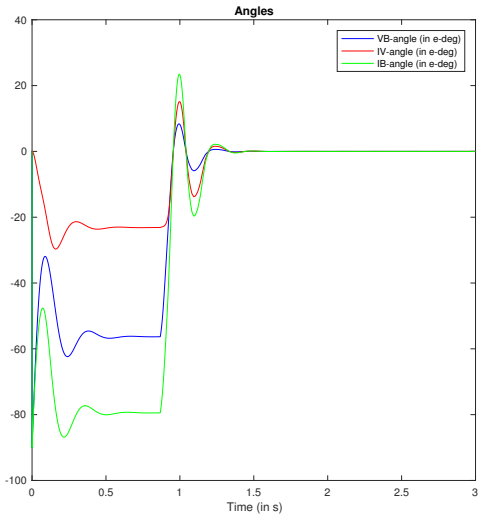

Figure 4.5: $K_p = 10,\ K_i = 1.4,\ K_d = 2$ and 192 u-steps/360 electrical

Chapter 5

Simulation

5.1 Graphical User Interface

For better, faster and easier handling of the simulations, a Graphical User Interface (GUI) is implemented. The GUI should behave in an understandable and predictable manner, so that a user knows what to expect when he or she performs an action. For example, when a mouse click occurs on a pushbutton, the GUI should initiate the action described on the label of the button. The GUI, illustrated on Figure 5.1, is composed of intuitive controls like editable fields to enter the value of a parameter, pushbuttons to execute an action, check boxes to select options, pop-up menus to choose among several choices, and so forth. As an example, the pushbutton *Open figure* allows to open the figure in a new window. In this new window, the user can add a cursor, zoom in, etc. These operations are not possible otherwise. It is also useful to be able to open different graphs in different windows in order to easily compare them.

The model has different options. Indeed, depending on what the user wishes, it can take into account an inductance, a frequency sweep, a cogging torque, and/or a torque shock. Moreover, the model can be runned in open-loop or in closed-loop. When a frequency sweep (linear increase of the speed of the voltage) is desired, a start rotation speed, an end rotation speed and an acceleration of the voltage need to be entered. As mentioned above, a table needs to be uploaded in order to take the cogging torque into account. This table should have the .mat format and be composed of two columns. The first one should contain the amplitude of the cogging torque and the second one the corresponding rotor positions. For the simulation of a torque shock with a sine cycle

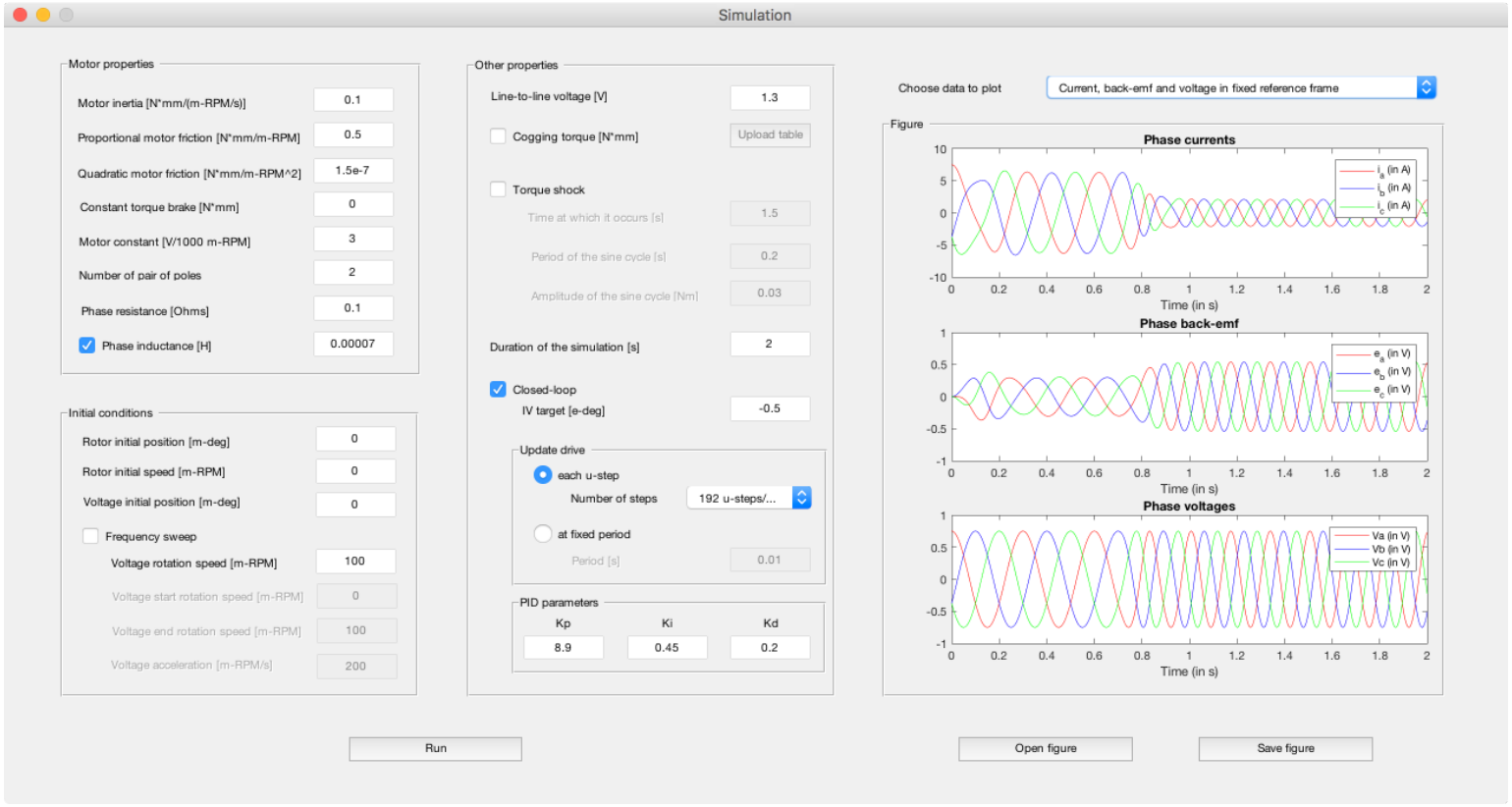

Figure 5.1: Graphical User Interface allowing to enter the specifications of the motor, to run the simulation and to plot the desired graph.

shape, an amplitude, a period and a time at which it occurs need to be mentioned. When the model is runned in closed-loop, the IV target and the PID parameters have to be chosen as well as the scenario:

- update drive at each u-step (selection of the number of u-steps/360 electrical: 6, 48 or 192),
- update drive at fixed period (choice of the period).

5.2 Results in Open-loop

Appendix B contains all the parameters used in the simulations presented in this section. The results exposed in subsections 5.2.1 to 5.2.6 are obtained by simulating the behavior of a BLDC motor having the parameters given in Table B.1 (Simulation 1). Concerning subsection 5.2.7, please refer to Table B.2 (Simulation 2). Table B.3 and Table B.4 (Simulation 3) give information about subsection 5.2.8. Finally, the simulation referred in subsection 5.2.9 is based on Table B.5 (Simulation 4).

5.2.1 Current, back-emf and voltage

Figures 5.2 and 5.3 respectively show the current, back-emf and voltage in fixed and rotating reference frames. In steady state, current, back-emf and voltage have a sinusoidal waveform in the fixed reference frame while they are constant in the rotating reference frame. Furthermore, Figure 5.3 shows that initially the back-emf is equal to zero, then increases with the increasing rotation speed of the rotor, oscillates a bit and finally stabilizes at a steady-state value. Meanwhile, the current decreases as the back-emf increases, and the other way around, to finally stabilize at its steady-state value. The applied voltage is constant all along. These behaviors fit the equations presented in Chapter 3.

Figure 5.4 shows the current in different reference frames (cf Section 2.3): firstly, the phase currents in the three-phase fixed reference frame; secondly, the α- and β-currents in the two-phase fixed reference frame; and finally, the direct and quadrature currents in the rotating reference frame. As expected, the currents in fixed reference frames exhibit a sinusoidal waveform while the currents in rotating reference frame are constant in steady-state. The direct and quadrature currents as well as the total

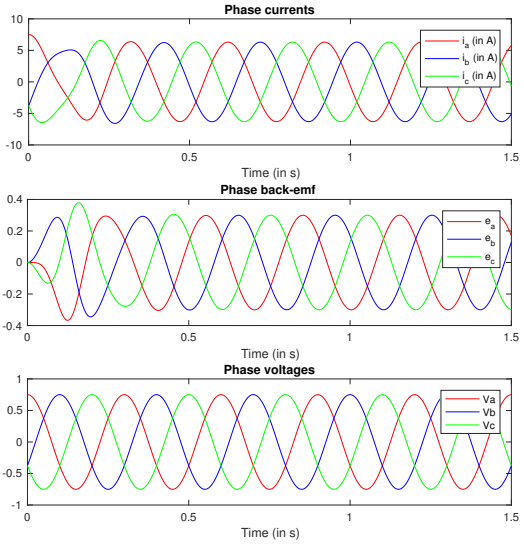

Figure 5.2: Current, back-emf and voltage in fixed reference frame.

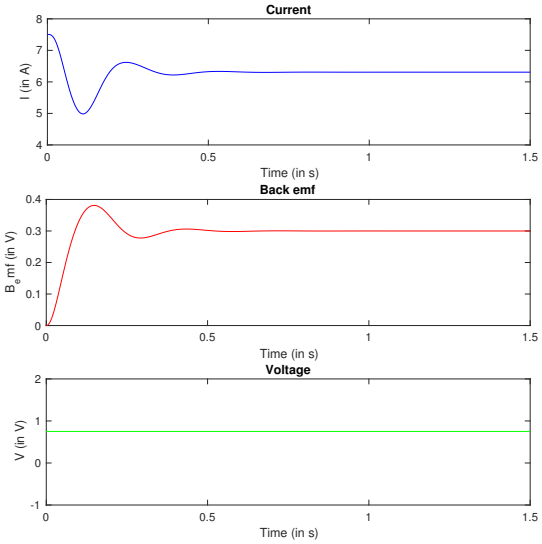

Figure 5.3: Current, back-emf and voltage in rotating reference frame.

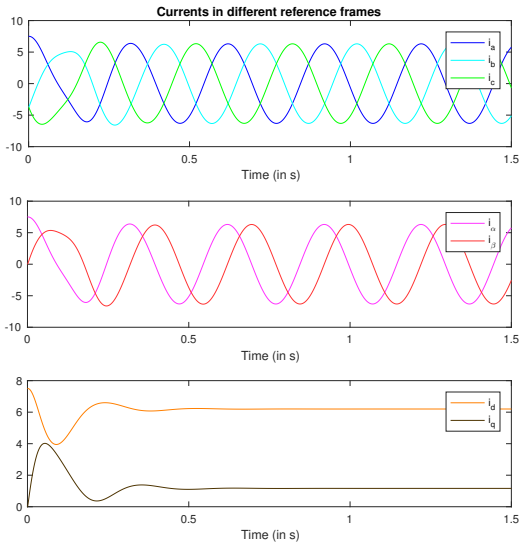

Figure 5.4: Current in different reference frames.

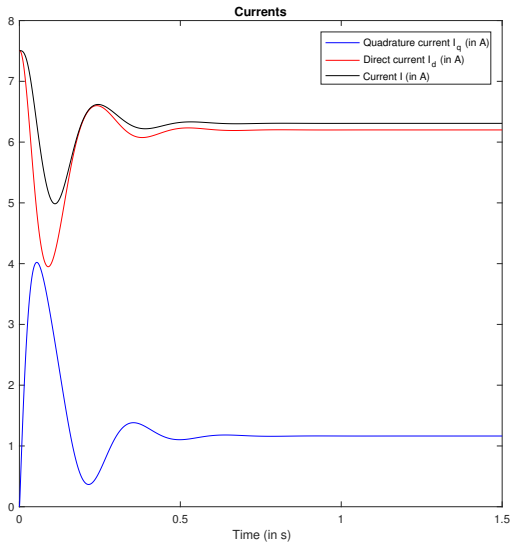

Figure 5.5: Direct and quadrature currents.

current are illustrated on Figure 5.5. This graph gives information on the efficiency of the motor. As only the orthogonal (quadrature) component produces torque, while the parallel (direct) component is useless, an efficient brushless motor drive will function so as to minimize the direct component and maximize the quadrature component. Indeed, the quadrature current component produces a field at right angles to the rotor magnet and therefore results in torque. Whereas the direct current component produces a field that is aligned with the rotor magnet and therefore produces no torque.

5.2.2 Position and speed of rotor and voltage

Figure 5.6 shows the position of the voltage and the rotor. This graph is useful to detect stalling, for example, as it is easy to see whether the rotor is following the voltage. From Figure 5.7, it can be seen that the rotation speed of the rotor is equal to the rotation speed of the voltage in steady-state. Moreover, according to (3.1), (3.2) and (3.3), the rotor speed and the back-emf have the same shape.

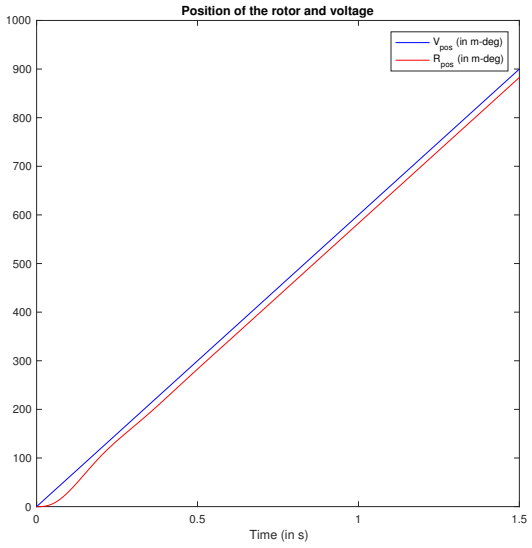

Figure 5.6: Position of rotor and voltage.

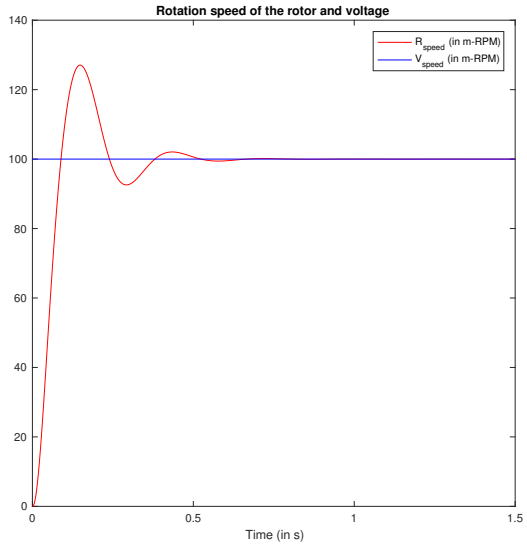

Figure 5.7: Rotation speed of rotor and voltage.

The rotation speed of the rotor can be computed by hand to convince us that it has the expected shape. Making the assumption that T_{drive} is constant and considering only the homogeneous differential equation and the frictional part of the mechanical torque,

it can be found that

$$J\frac{d\omega}{dt} + Fr2_m\omega^2 + Fr_m\omega = 0 \tag{5.1}$$

$$\omega(t) = \frac{cFr_m \exp(\frac{Fr_m}{J}t)}{1 + cFr2_m \exp(\frac{Fr_m}{J}t)} \tag{5.2}$$

We notice that the dynamics depends on the parameters J, Fr_m and $Fr2_m$. Here c is the constant of integration. This corresponds to the results obtained on Figure 5.7.

5.2.3 Torques

The acceleration torque together with the mechanical torque and the driving torque are illustrated on Figure 5.8. Figure 5.9 shows the different components of the mechanical torque. Here, only the frictional torque is taking into account.

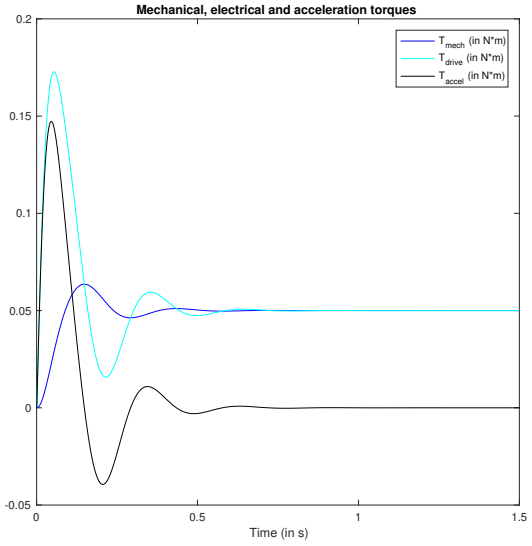

Figure 5.8: Acceleration torque.

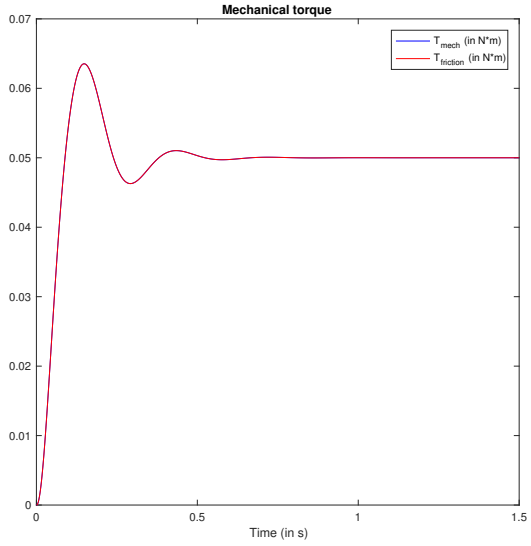

Figure 5.9: Mechanical torque.

In steady-state, when the rotor speed is stabilized (rotor acceleration, Ω, equals zero), the mechanical torque is equal to the driving torque. Indeed, from (2.9),

$$\Omega = \frac{T_{drive} - T_{mech}}{J} = 0 \tag{5.3}$$

therefore

$$T_{drive} = T_{mech} \tag{5.4}$$

and

$$T_{accel} = 0 \tag{5.5}$$

Notice that according to (3.11), the electrical torque and the quadrature current have the same shape. Furthermore, considering only the frictional torque, $T_{mech} = T_{friction}$, and according to (3.8), the frictional torque is linked to the rotational speed ω.

5.2.4 VB-, IV-, and IB-angles

VB-, IV- and IB-angles (Figure 5.10) give a lot of useful information, especially on the efficiency of the motor.

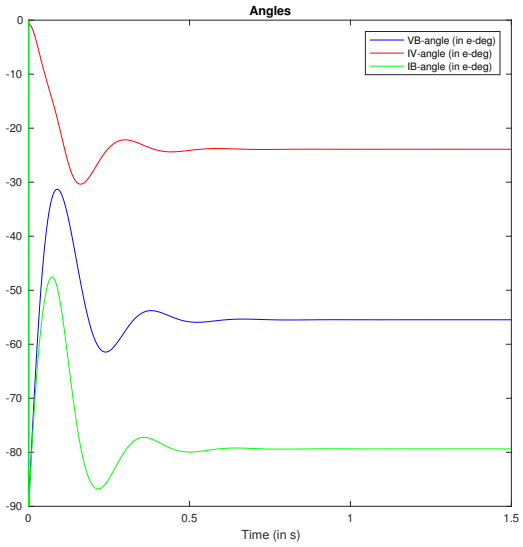

Figure 5.10: VB-, IV-, and IB-angles.

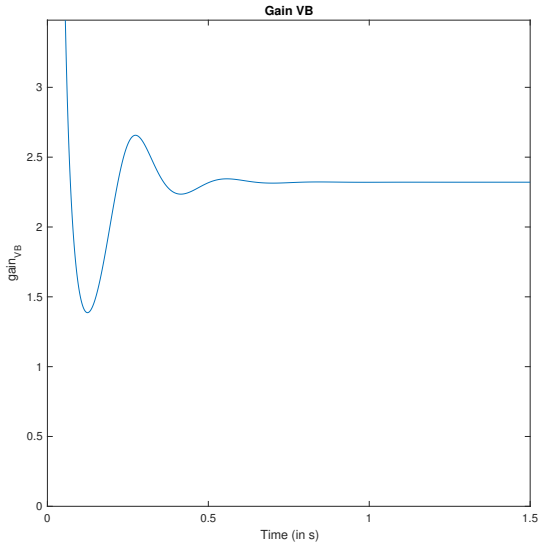

Figure 5.11: Gain VB.

The IB-angle gives information on the efficiency and the driving torque. Indeed, if IB-angle $= -90$, it means that the driving torque is equal to zero as in this case $I = I_d$ and $I_q = 0$, and the motor drive is totally inefficient. Contrariwise, if IB-angle $= 0$, then $I = I_q$ and $I_d = 0$, the motor is driven very efficiently and the driving torque is at its maximal value. This is valid in all cases, either the inductance is taken into account or neglected.

A similar thinking can be carried out with IV- and VB-angles but here, two cases must be distinguished: when the inductance is taken into account or when it is neglected. In the latter case, IV-angle = 0 or VB-angle = 0 means the motor is driven in the most efficiently way while IV-angle $\neq 0$ or VB-angle $\neq 0$ means a totally inefficient drive of the motor. However, if the inductance is not negligeable, the most efficient drive of the motor does not occur anymore when IV- and VB-angles are exactly equal to zero, but when they are slightly different from zero.

The VB gain (Figure 5.11) is defined as

$$\text{gain}_{VB} = \frac{\text{VB-angle}}{\text{IV-angle}} \tag{5.6}$$

It is an important variable to know. In fact, as it is common to measure the IV-angle, once the VB-gain is known, the VB-angle can be obtained as:

$$\text{VB-angle} = \text{IV-angle} \cdot \text{gain}_{VB} \tag{5.7}$$

5.2.5 Electromechanical power balance

Figure 5.12 shows that the driving power is equal to the mechanical power. The driving power is defined as

$$P_{drive} = i_a e_a + i_b e_b + i_c e_c \tag{5.8}$$

while the mechanical power is defined as

$$P_m = T_{drive} \cdot \omega \tag{5.9}$$

where $T_{drive} = K_i \cdot \frac{3}{2} i_q$. Nevertheless, according to (2.8) and (3.11), if everything is expressed in the right units, it is obvious that $P_{drive} = P_m$. It is however important to note that the driving power is not equal to the electrical power. While the driving power is defined as the sum on each phase of the product of the current by the back-emf, the electrical power is defined as the sum on each phase of the product of the current by the voltage. In theory, if there is no losses at all, these two powers are equal, and therefore, mechanical and electrical powers are also identical in steady-state. In pratice, there are always losses, and the mechanical power P_m is not equal to the electrical power P_e. In

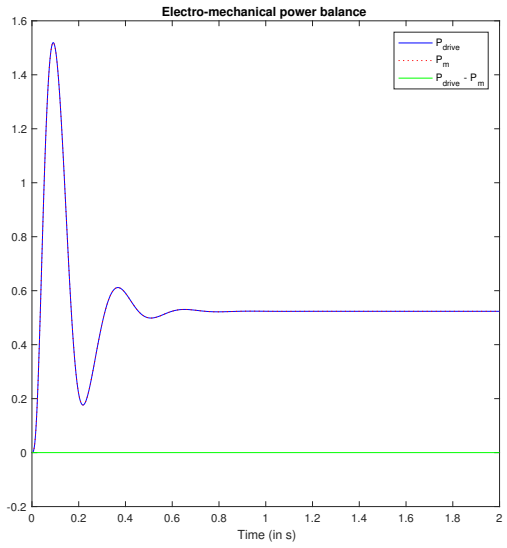

Figure 5.12: Electromechanical power balance.

this case, the efficiency of the motor is given by the ratio of the mechanical power to the electrical power: $\eta = \frac{P_m}{P_e}$.

5.2.6 Phasor diagram GUI

Figure 5.13 shows the phasor diagram of the motor. By sliding the cursor, the time evolution can be visualized. This figure is plotted in order to check that the simulation is consistent. On the right part of the figure, the relative position of the rotor and the voltage can be seen as well as the direction of the back-emf and the losses $R \cdot I$. The figure on the left however gives information on the rotation of the rotor; the mechanical angle of the rotor can be read from this figure.

The phasor diagram is a valid representation for sinusoidal function, and can therefore be used when the inductance is neglected. The general equation (2.1) is simplified as follows:

$$V = RI + E \tag{5.10}$$

where the term $L\frac{dI}{dt}$ has been neglected.
When the inductance is taken into account, the assumption of sinusoidal waveform cannot be made anymore. Indeed, the variation of currents does not only depend on

the rotation speed of the rotor, there are second order effects, such as current variations due to cogging torque.

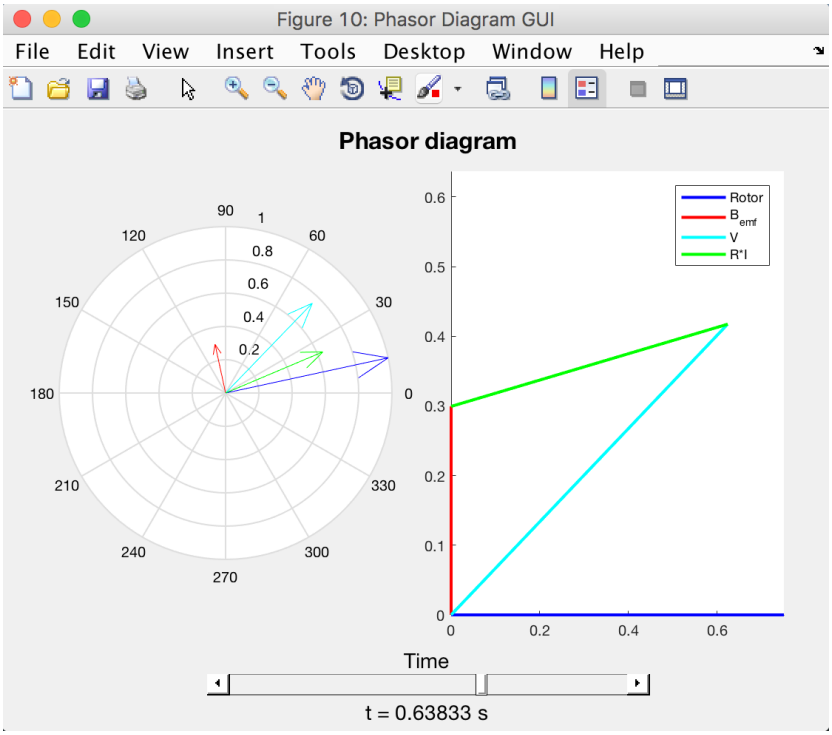

Figure 5.13: Graphical User Interface allowing to visualize the phasor diagram at the selected time.

From the figure, one sees on the one hand that there is a phase shift of 90 degrees between the rotor and the back-emf as mentionned in Section 3.1, and on the other hand, that the rotor is behind the voltage. In fact, the rotor tries to follow the voltage. In steady state, the rotation speed of the rotor is equal to that of the voltage. However, the rotor position is always a bit lower than that of the voltage. Indeed, the magnetic pole of the rotor is trying to follow the rotating magnetic field of the stator, due to the "rotation of the voltage".

5.2.7 Frequency sweep

As shown on Figure 5.14, the model allows to linearly increase the rotation speed of the voltage at start-up. The voltage rotation speed starts at a given speed, then increases with a certain acceleration until reaching another speed. These three parameters can be entered in the GUI.

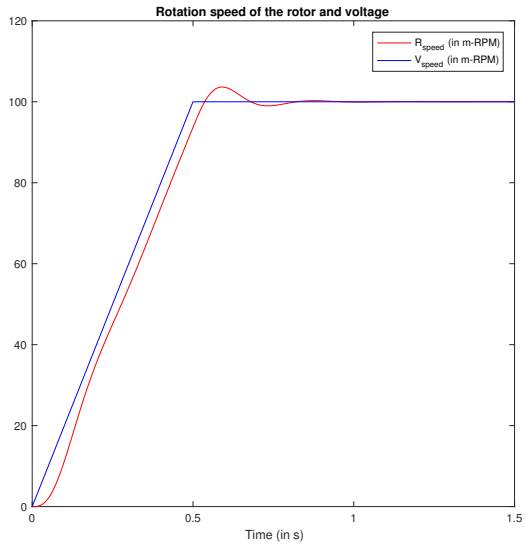

Figure 5.14: Speed of rotor and voltage with a frequency sweep.

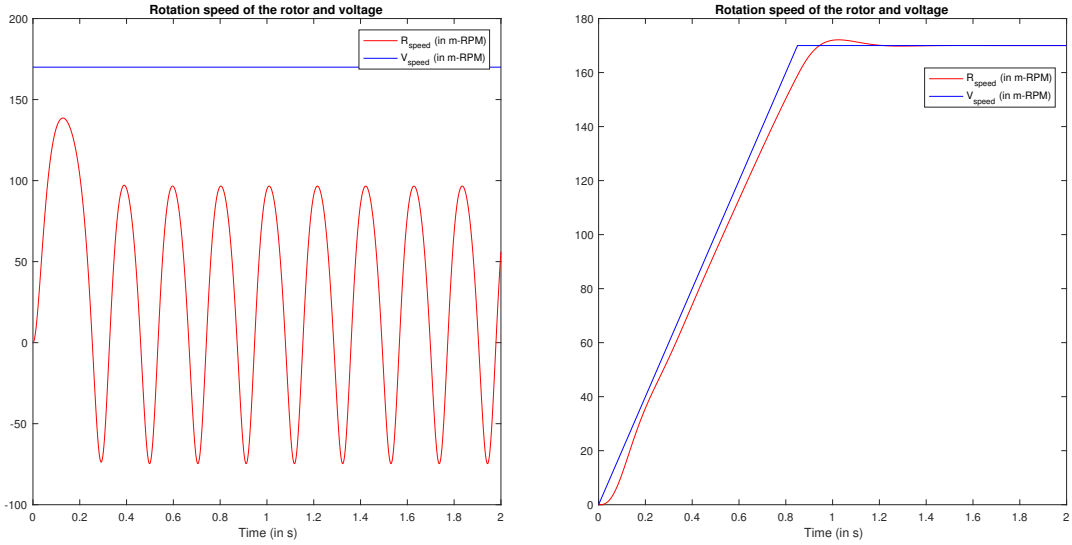

(a) Without frequency sweep.

(b) With frequency sweep.

Figure 5.15: Rotation speed of rotor and voltage.

From the graph (Figure 5.14), one can conclude that starting the motor with a frequency sweep leads to less oscillations, and hence less noise. Moreover, the frequency sweep allows to reach higher rotation speed because it avoids early stalling at start-up time. This is illustrated on Figure 5.15. On the left, the motor is driven without frequency sweep with a voltage rotation speed of 170 m-RPM. Obviously, the rotor cannot keep-up with this speed and stalling occurs. On the right, the voltage rotation speed is increased from 0 to 170 m-RPM with an acceleration of 200 m-RPM/s. All other parameters of the simulation are retained. In this case, one sees that the rotor is able to reach the 170 m-RPM.

5.2.8 Cogging torque

Let us recall that the cogging torque is position dependent but the modelling of this torque is not the concern of this work. Therefore, a table listing the measurements of the cogging torque as a function of the mechanical position of the rotor, $T_{cog}(\theta_m)$, over one revolution of 360 degrees has to be uploaded into the GUI (cf. Table B.4). Then a spline interpolation is performed in order to get the value of the cogging torque at each desired rotor position. This way, it can be taken into account in the model: it is simply added to the frictionnal torque and possibly to the torque shock in order to compute the mechanical torque. Figure 5.16 shows the shape of the mechanical torque when a cogging torque is taken into account. Note that some small oscillations also appear in the frictional torque as it depends on the rotation speed of the rotor which is itself affected by the cogging torque (it can be seen on Figure 5.17). Finally, on the figure, it is clear that the mechanical torque is the sum of the frictional torque and the cogging torque. Figure 5.18 shows the cogging torque as a function of the time, the position of the rotor and finally the Fourier transform of the cogging torque. As can be seen on the second subplot, there are approximately 24 cycles over 360 degrees. Therefore, the main frequency of the cogging torque should be 24 times higher than the rotation speed of the rotor. This is verified on the third subplot. Indeed, the main frequency is equal to 2399 which is almost equal to $24 \cdot 100$ m-RPM $= 2400$ m-RPM, where 100 m-RPM is the rotation speed of the motor.

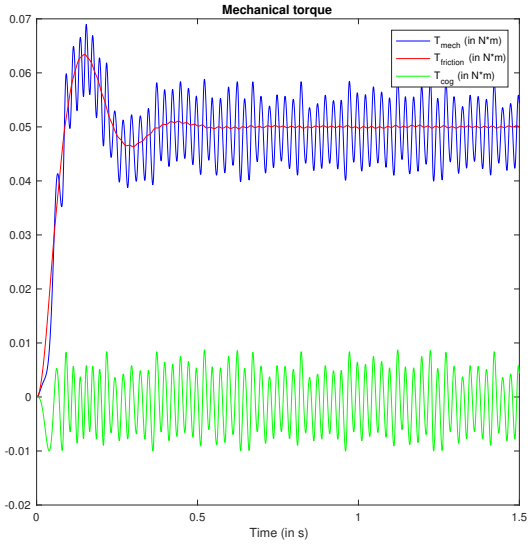

Figure 5.16: Mechanical torque with a cogging torque.

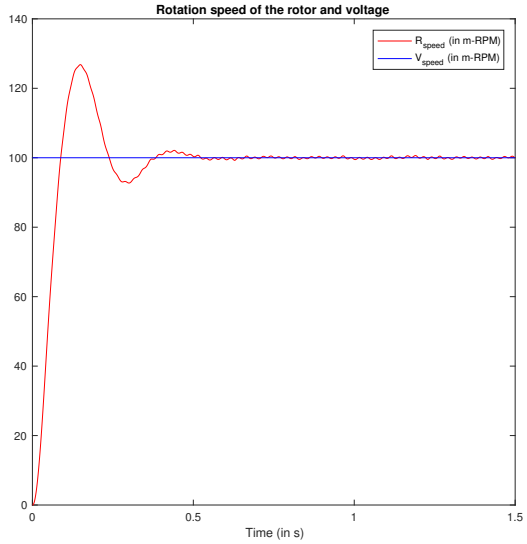

Figure 5.17: Speed of rotor and voltage with a cogging torque.

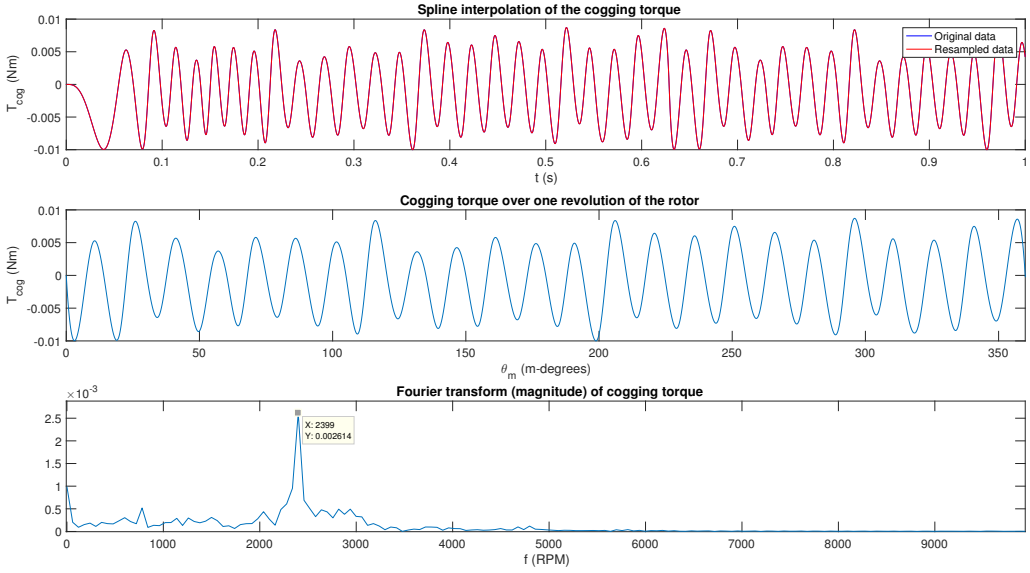

Figure 5.18: Cogging torque and Fourier transform.

5.2.9 Torque shock

Figure 5.19 shows the mechanical torque when a torque shock is applied. The torque shock is modelled as a sine cycle of chosen amplitude and period, appearing at a desired time. In the same way as for the case of the cogging torque, oscillations also appear in the frictional torque as it depends on the rotation speed of the rotor which is itself affected by the torque shock.

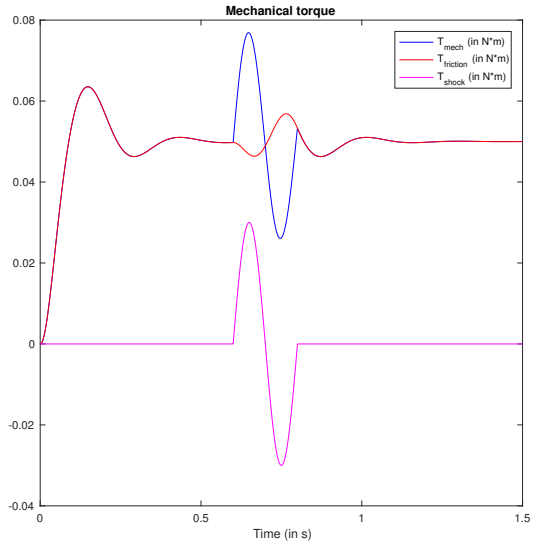

Figure 5.19: Mechanical torque with a torque shock.

5.3 Results in Closed-loop

In closed-loop, the same graphs as in open-loop can be plotted. Some of them are illustrated on Figure 5.20. One clearly sees on those graphs that the motor starts in open-loop, and as soon as steady-state is reached, the regulation begins.

Subfigure 5.20d shows that the IV target is zero and that the inductance is neglected during this simulation as the three angles are simultaneously equal to zero. Moreover, the motor drive is efficient as the direct current is zero (subfigure 5.20c).

Subfigure 5.20h shows that the output power is increased with the regulation. This is consistent as both the driving torque (subfigure 5.20g) and the rotation speed (subfigure 5.20f) are greater (let's recall that the mechanical power is given by $P_m = T_{drive} \cdot \omega$). The driving torque is itself bigger as the quadrature current is increased

(subfigure 5.20c). The rise of the voltage's rotation speed is a direct consequence of the regulation as it is the output of the PID controller.

On subfigures 5.20a and 5.20b, one sees that the back-emf is increased as a consequence of the rise of the rotation speed and the amplitude of the current is decreased.

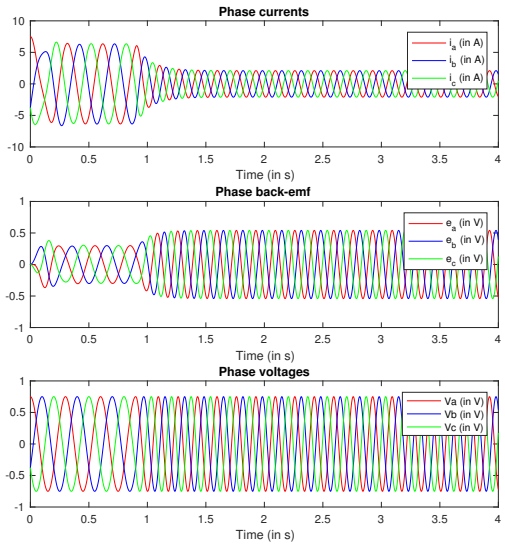

(a) Current, back-emf and voltage in fixed reference frame.

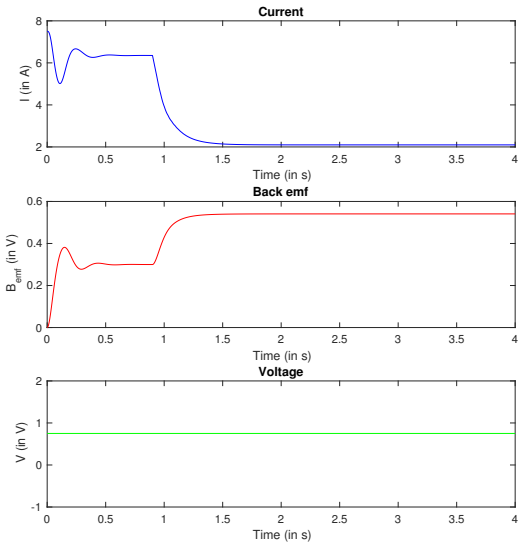

(b) Current, back-emf and voltage in rotating reference frame.

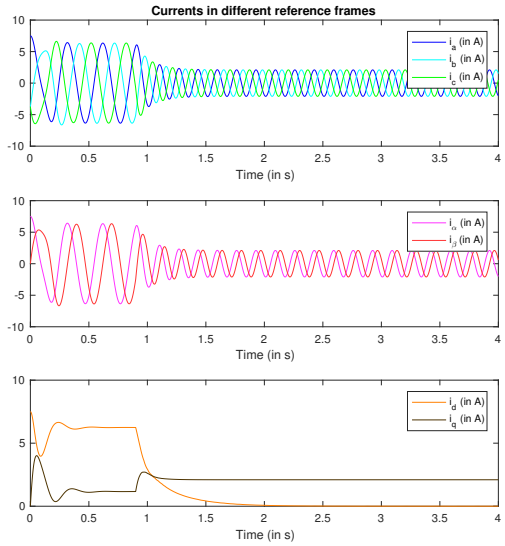

(c) Current in different reference frames.

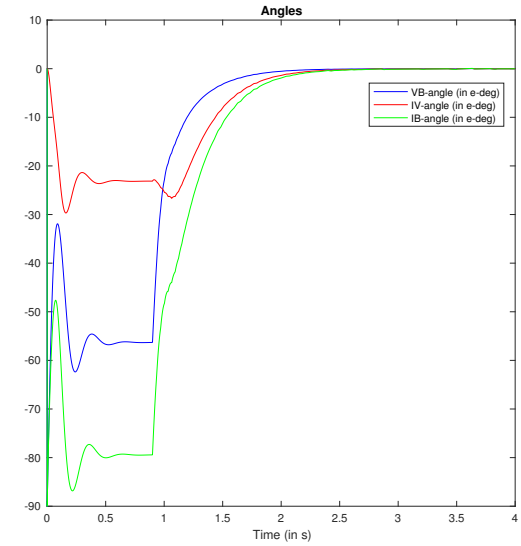

(d) VB-, IV-, and IB-angles.

Figure 5.20: Results of the simulation in closed-loop.

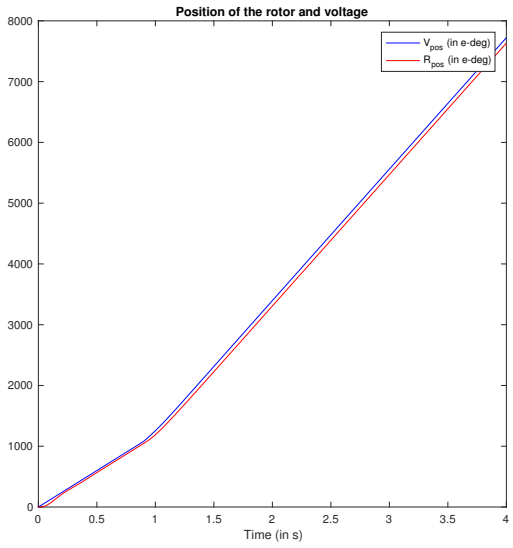

(e) Position of rotor and voltage.

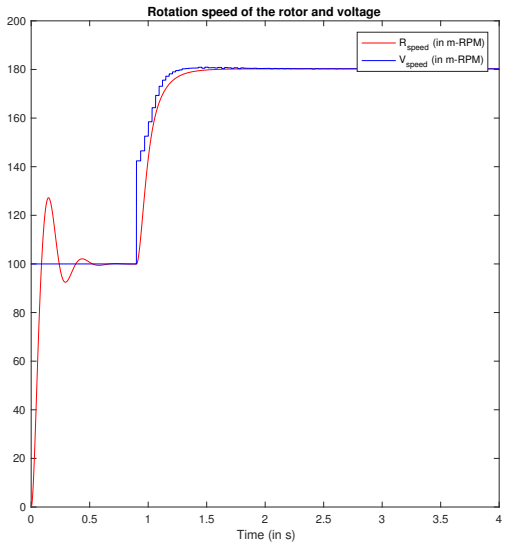

(f) Rotation speed of rotor and voltage.

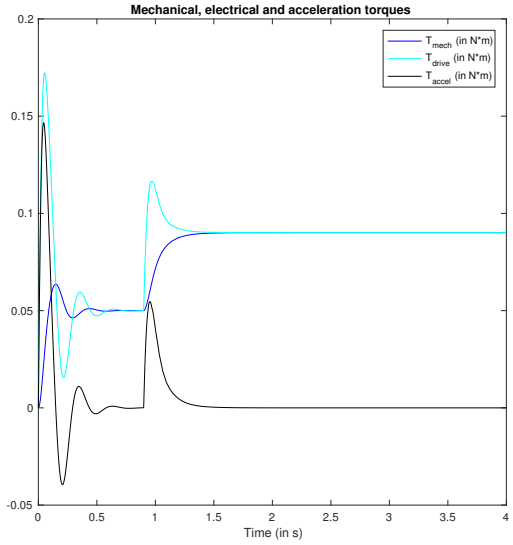

(g) Acceleration torque.

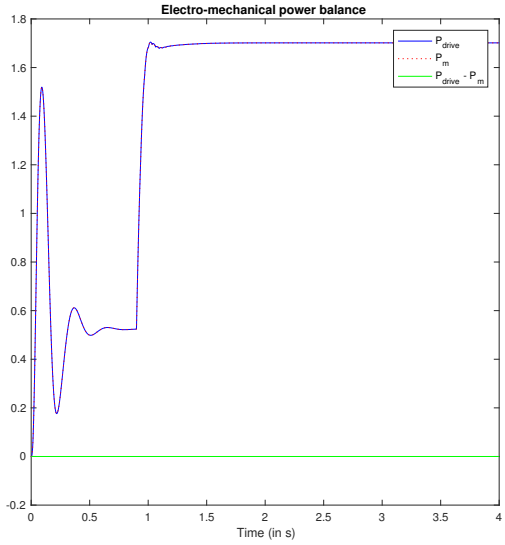

(h) Electromechanical power balance.

Figure 5.20: Results of the simulation in closed-loop. (cont.)

Chapter 6

Open-loop electrical system characterization

The modeling of BLDC motors described before requires the setting of motor parameters for its proper functioning. This chapter deals with the extraction of electrical parameters from test measurements. The proposed techniques determine the stator resistance R, the inductance L, the electrical motor constant (or back-emf constant) K_e and the number of pole pairs p.

6.1 Motor pole pairs

The motor pole pairs parameter defines a ratio between mechanical and electrical quantities (mechanical vs electrical rotor position/speed). The method [2] requires to spin the motor by an external driving motor at a constant speed and to measure the generated voltage frequency f (electrical speed). Then, by measuring the speed of the motor ω (mechanical speed), the motor pole pairs can be computed using the equation given below.

$$p = \frac{60 f[Hz]}{\omega[rpm]} \tag{6.1}$$

The result should be very close to an integer number.

Example 6.1.1. *Based on Figure 6.1, and knowing that the mechanical rotation speed of the motor is 100 m-RPM, the motor pole pairs parameter is computed as follows:*

$$p = \frac{60f}{\omega} = \frac{60}{\omega\, T_{el}} = \frac{60}{100 \times (1.779 - 1.479)} = 2$$

where T_{el} is the period of the measured signal.

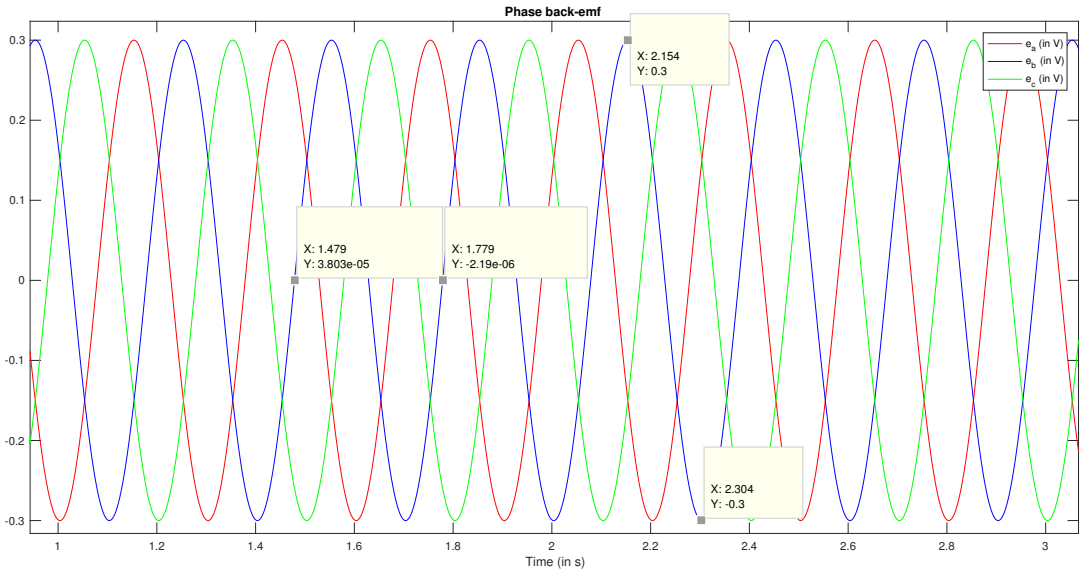

Figure 6.1: Graph of the three-phase back-emf voltage over time, corresponding to a three-phase measurement of the generated phase voltage of a motor spinned by an external driving motor.

6.2 Back-emf constant

The back-emf constant K_e can be obtained by measuring the no-load line-to-line voltage V_{pk} of the motor while it is driven through the shaft at a constant speed as illustrated on Figure 6.2. The constant K_e gives a ratio between back-emf voltage and the angular electrical frequency/speed.

The steps below must be followed in order to compute the back-emf constant [2]:

1. Spin the motor by an external driving motor at a constant speed. Higher speed is preferred, because the voltage measurement error is lower.

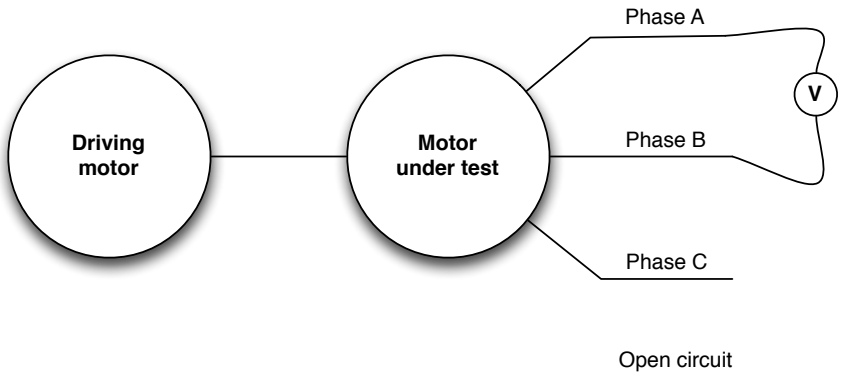

Figure 6.2: Measurement of the no-load line-to-line voltage for the determination of the back-emf constant.

2. Measure the generated line-to-line voltage.

3. Calculate the back-emf constant according to (6.2). Depending on the units of ω, K_e can be expressed as [V/ rad/s], or more commonly as [V/m-RPM].

$$K_e = \frac{V_{pk}}{\sqrt{3}\,\omega} = \frac{V_{pk-pk}}{2\sqrt{3}\,\omega} \tag{6.2}$$

Example 6.2.1. *Still based on Figure 6.1, the back-emf constant can be determined in the following way:*

$$K_e = \frac{V_{pk-pk}}{2\,\omega} = \frac{V_{pk-pk}\,T_{el}}{2 \times 2\pi} = \frac{V_{pk-pk}\,T_{el}}{4\pi} \left[\frac{V\ s}{rad}\right]$$

or more commonly,

$$\begin{aligned} K_e &= \frac{V_{pk-pk}\,T_{el}}{4\pi} \times \frac{2\pi}{60} \times pp \times 1000 \\ &= \frac{(0.6) \times (1.779 - 1.479)}{4\pi} \times \frac{2\pi}{60} \times 2 \times 1000 \\ &= 3 \left[\frac{V}{1000\ m\text{-}rpm}\right] \end{aligned}$$

where V_{pk-pk} is in this example the peak-to-peak phase voltage (line-to-line voltage is $\sqrt{3}$ times bigger than the phase voltage).

6.3 Resistance and inductance of the motor

The electrical parameters R, L and K_e can actually be computed using equations directly derived from the phasor diagram illustrated on Figure 6.3:

$$V\cos(IV) = K_e\,\omega\cos(IB) + Ri \tag{6.3}$$

$$V\sin(IV) = K_e\,\omega\sin(IB) + (\omega \times \frac{2\pi}{60} \times p)Li \tag{6.4}$$

where K_e is expressed as [V/m-rpm], ω as [m-rpm] and $K_e\,\omega$ is the back-emf. IV and IB are respectively the IV- and IB-angles. Moreover, there is a relationship linking the three angles: $IB = IV + VB$.

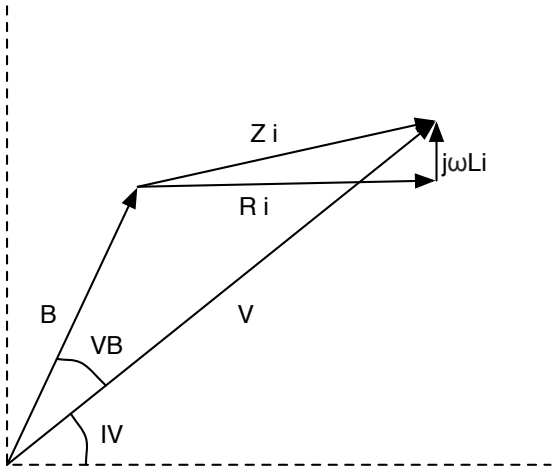

Figure 6.3: Phasor diagram of the motor.

Based on these equations, the three parameters can be determined through two tests where IV- and IB-angles as well as the peak current are measured for two different values of the voltage amplitude and frequency. This method works fine in theory. However, in pratice, while IV-angle can be measured, IB- and VB-angles cannot. Since IB-angle is unknown, this method is unusable and approximations need to be made.

6.3.1 Approximate method

A method based on assumptions needs to be derived in order to determine the resistance R and the inductance L, since K_e can be measured using an other test measurement (see Section 6.2). The difficulty here is to find an assumption which leads to the smallest possible error on the values of R and L.

The closed-loop model shows that IV-, IB- and VB-angles become really small as the motor is driven more efficiently. For this purpose, the voltage can be decreased. Indeed, the voltage leading to the most efficient drive is the one just before losing synchronization of the system, i.e. before the stalling. With such a voltage amplitude, it can be shown that while all angles are close to zero, VB-angle is always smaller than IB-angle, and it can therefore be approximated to zero with a small error.

Hence making the assumption that the back-emf is aligned with the voltage, i.e. $VB = 0$ so that $IB = IV$, the phasor diagram becomes as illustrated on Figure 6.4, leading to the following equations:

$$R = \frac{V\cos(IV) - K_e\,\omega\cos(IV)}{I_{pk}} \quad [\Omega] \tag{6.5}$$

$$L = \frac{V\sin(IV) - K_e\,\omega\sin(IV)}{2\pi\,\frac{\omega}{60}\,p\,I_{pk}} \quad [H] \tag{6.6}$$

where ω is expressed in [m-RPM] and K_e in [V/m-RPM].
The inductance can also be computed using the equation given below.

$$L = \frac{R\tan(IV)}{2\pi\,\frac{\omega}{60}\,p} \quad [H] \tag{6.7}$$

In conclusion, in order to compute the resistance and the inductance of the motor, the method requires to follow the steps below:

1. Start the motor with a high[1] voltage and wait for steady-state.

2. Spin the motor in open-loop and decrease gradually the voltage amplitude, maintaining a constant speed all along, until the motor looses synchronization, i.e.

[1]The voltage is sufficiently high so that stalling does not occur during startup time.

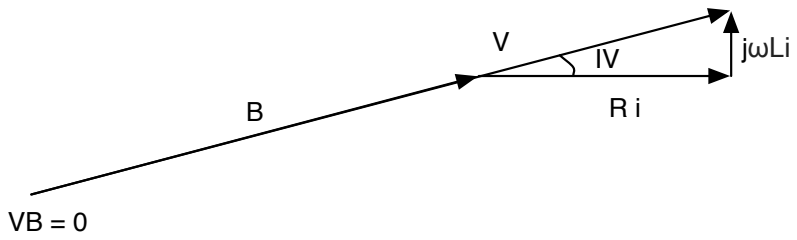

Figure 6.4: Phasor diagram of the motor where the back-emf is aligned with the voltage.

stalling occurs. Higher speeds are preferred so that the effect of the inductance cannot be neglected.

3. Spin the motor at the speed previously chosen with the smallest observed voltage which does not lead to stalling, and measure the peak current as well as the IV-angle.

4. Calculate the resistance according to (6.5).

5. Calculate the inductance according to (6.7).

Example 6.3.1. *A GUI has been implemented in order to perform the first 3 steps using a simulation based on the model previously implemented. Indeed, as it can be seen on Figure 6.5, once steady-state is reached, the voltage can be decreased by a chosen voltage step, and the simulation can be stopped when stalling occurs. For this purpose, signals are plotted in real-time.*

Using this simulation, the values from Table 6.1 are obtained. Based on these ones, and knowing from Sections 6.1 and 6.2 that the number of pole pairs is 2 and the back-emf constant is 3 V/1000 m-rpm, the resistance and the inductance can be computed. The resistance is then equal to

$$\begin{aligned} R &= \frac{V\cos(IV) - \frac{K_e}{1000}\,\omega\cos(IV)}{I_{pk}} \\ &= \frac{0.6245\cos(0.5424) - \frac{3}{1000}\,150\cos(0.5424)}{1.746} \\ &= 0.0999\ [\Omega] \end{aligned}$$

and the inductance is

$$\begin{aligned} L &= \frac{R\tan(IV)}{2\pi\,\frac{\omega}{60}\,p} \\ &= \frac{0.0999\tan(0.5424)}{2\pi\,\frac{150}{60}\,2} \\ &= 3\cdot 10^{-5}\ [H] \end{aligned}$$

This is an approximate method. Therefore, there is an error related to the assumptions used. Indeed, VB-angle is assumed to be equal to zero while in reality, it is equal to 0.7006 e-deg. Knowing that the resistance and the inductance are actually equal to $0.1\,\Omega$ *and* $7\cdot 10^{-5}$ *H, the error related to both can be computed.*

$$error_R = \frac{|R-\hat{R}|}{|R|} = \frac{|0.1-0.0999|}{|0.1|} = 0.1\%$$

$$error_L = \frac{|L-\hat{L}|}{|L|} = \frac{|7\cdot 10^{-5}-3\cdot 10^{-5}|}{|7\cdot 10^{-5}|} = 57\%$$

where $\hat{R}$ *and* $\hat{L}$ *are the approximate values.*

Variables	Values	Units
ω	150	m-rpm
V	0.6245	V
IV	0.5424	e-deg
I_{pk}	1.746	A

Table 6.1: Measurements based on simulation for the determination of R and L parameters.

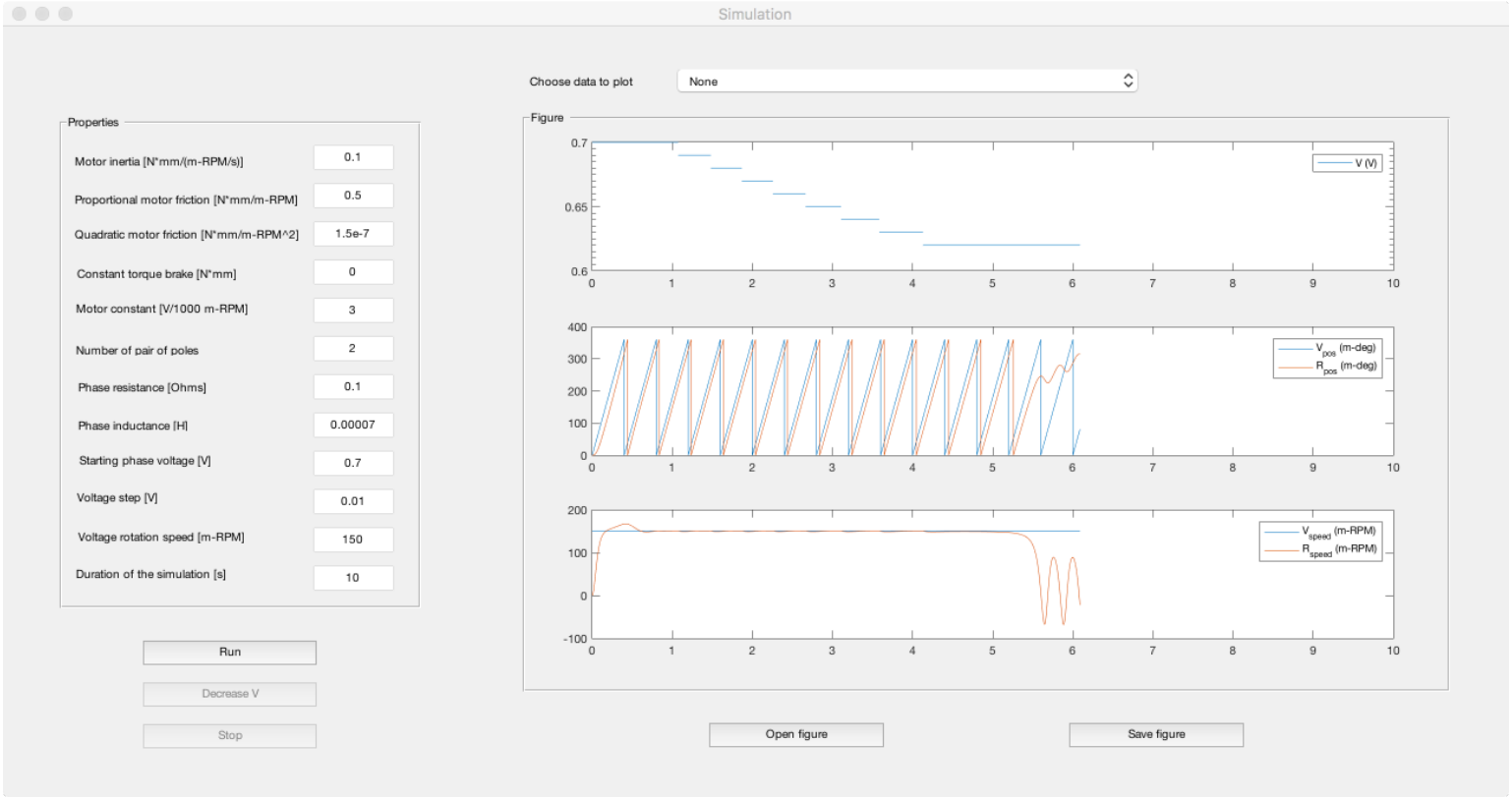

Figure 6.5: GUI allowing the open-loop electrical characterization.

Chapter 7

Open-loop mechanical system characterization

In order to run the model described above, motor electrical parameters as well as motor mechanical parameters are needed. This chapter deals with the extraction of mechanical parameters from test measurements. Method for calculating the inertia J of the system and the friction torque T_f are derived.

7.1 Friction parameter

The friction coefficient R_f defines the ratio between the friction torque and the angular velocity ($T_f = R_f\omega$). The method requires to run the motor at constant speed and to measure the quadrature current. Then, assuming that the motor constant K_T is known, the friction parameter can be computed using the equation given below.

$$R_f = \frac{K_T \frac{3}{2} i_q}{\omega} \tag{7.1}$$

Indeed, at constant speed ($\frac{d\omega}{dt} = 0$), the electromagnetic torque $T = K_T \frac{3}{2} i_q$ becomes

$$T = J\frac{d\omega}{dt} + T_f = R_f\,\omega$$

leading to (7.1).

Example 7.1.1. *Measuring i_q and computing the corresponding electromagnetic torques at different angular speeds provide more accurate results. By doing so, the graph on Figure 7.1 is obtained. A linear interpolation is performed leading to*

$$R_f = 0.5\,[Nmm/m\text{-}RPM]$$

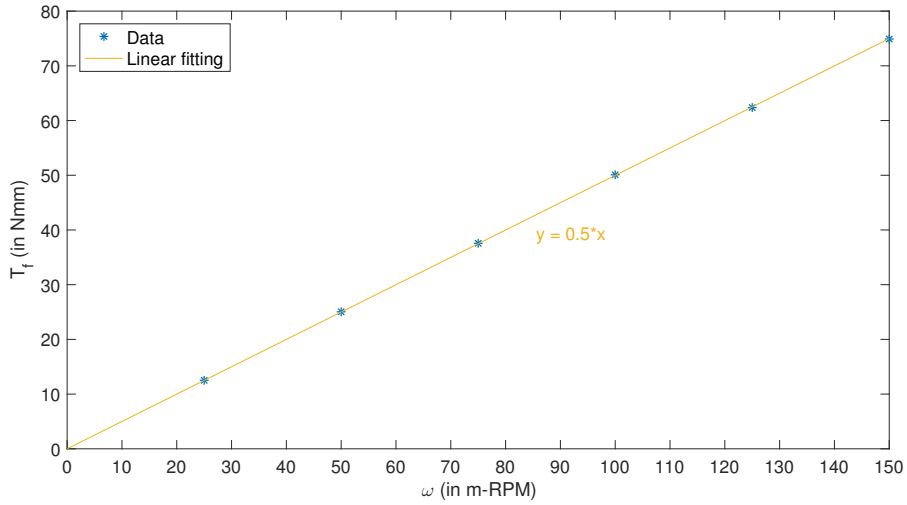

Figure 7.1: Friction torque measured at different angular velocities to identify friction parameter constant R_f.

Example 7.1.2. *In the case of motors for which the relationship between the friction torque and the angular speed cannot be approximated as linear but rather quadratic*

$$T_f = Fr2_m\,\omega^2 + Fr_m\,\omega,$$

a quadratic interpolation can be perfomed. Based on Figure 7.2, it gives the following results:

$$Fr2_m = 0.05\,[Nmm/m\text{-}RPM^2]$$
$$Fr_m = 0.3\,[Nmm/m\text{-}RPM]$$

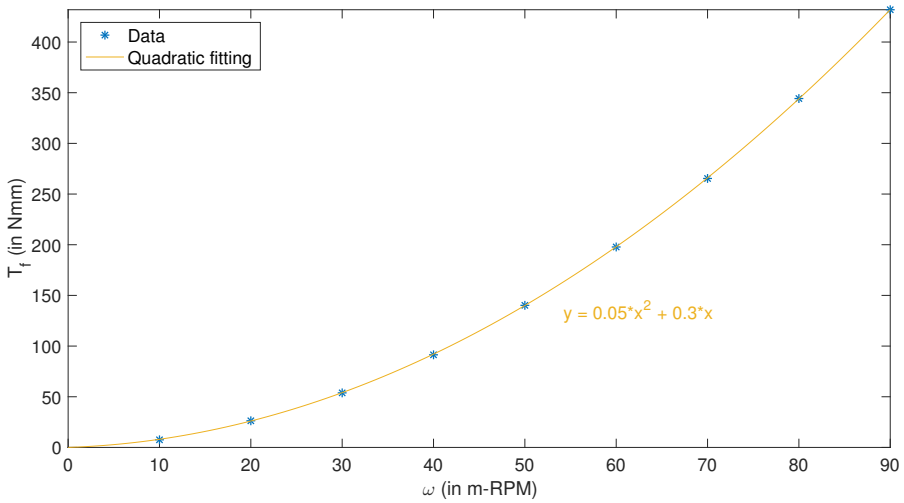

Figure 7.2: Friction torque measured at different angular velocities to identify friction parameter constants $Fr2_m$ and Fr_m.

7.2 Inertia

Inertia is the tendency of the motor to resist changes in its state of motion. The greater the inertia of the motor, the greater the torque required to rotate it. The method to determine the inertia consists in applying a step angular speed from ω_1 to ω_2 and measuring the time Δt required to achieve the new speed ω_2. Then, from the torque T needed for this change of speed, the inertia can be computed using the equation below.

$$J = \frac{T}{\Delta\omega/\Delta t} = \frac{K_T \frac{3}{2}\Delta i_q}{\Delta\omega/\Delta t} \tag{7.2}$$

This equation is obtained using the mechanical equation of the motor (7.3) and assuming that the friction torque can be neglected in transient state, i.e. during the change of speed, and perfoming a discretization of the derivative.

$$T = J\frac{d\omega}{dt} + T_f \tag{7.3}$$

The more linear is the change of speed, the more accurate the inertia obtained using (7.2) is. Therefore, a lower voltage is preferred to induce a smoother change.

Example 7.2.1. *Based on Figure 7.3 and Figure 7.4, and knowing that the motor constant K_e is equal to 3 V/(1000*m-RPM), the inertia is computed as follows:*

$$J = \frac{K_T \frac{3}{2}\Delta i_q}{\Delta\omega/\Delta t} = \frac{K_e \frac{60}{2\pi}\frac{3}{2}\Delta i_q}{\Delta\omega/\Delta t}$$

$$= \frac{3\frac{60}{2\pi}\frac{3}{2}(1.164 - 0.4654)}{\frac{100-40}{2.775-2.5}}$$

$$= 0.1376\,[Nmm/(m\text{-}RPM/s)]$$

The inertia is actually equal to 0.1 Nmm/(m-RPM/s). Therefore, there is a small error but this method gives a good first approximation.

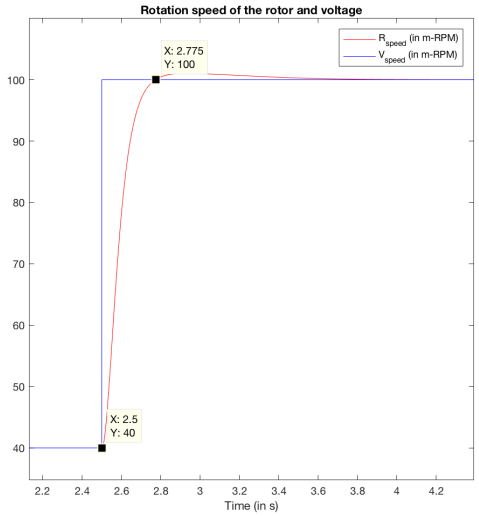

Figure 7.3: Angular speed of the motor when a step is applied.

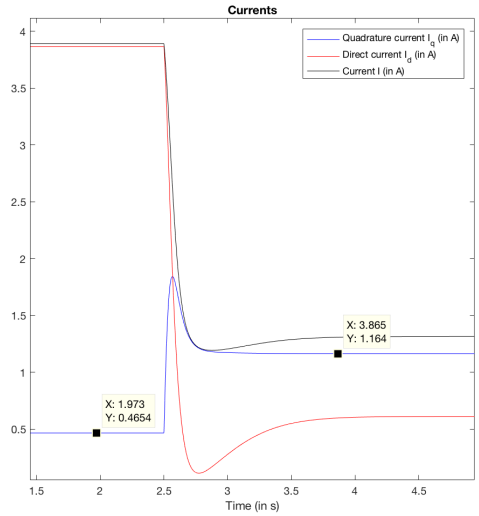

Figure 7.4: Evolution of the quadrature current under a step angular speed.

For the purpose of this example, a GUI has been implemented in order to perform an angular speed step. The GUI is visible on Figure 7.5. The starting and the final voltage's rotation speeds can be selected as well as the time at which the step has to occur. In this way, the behavior of the motor following a angular speed step can be analyzed, and the measurements required for the identification of the inertia can be performed (since measurements on real motor systems were unavailable).

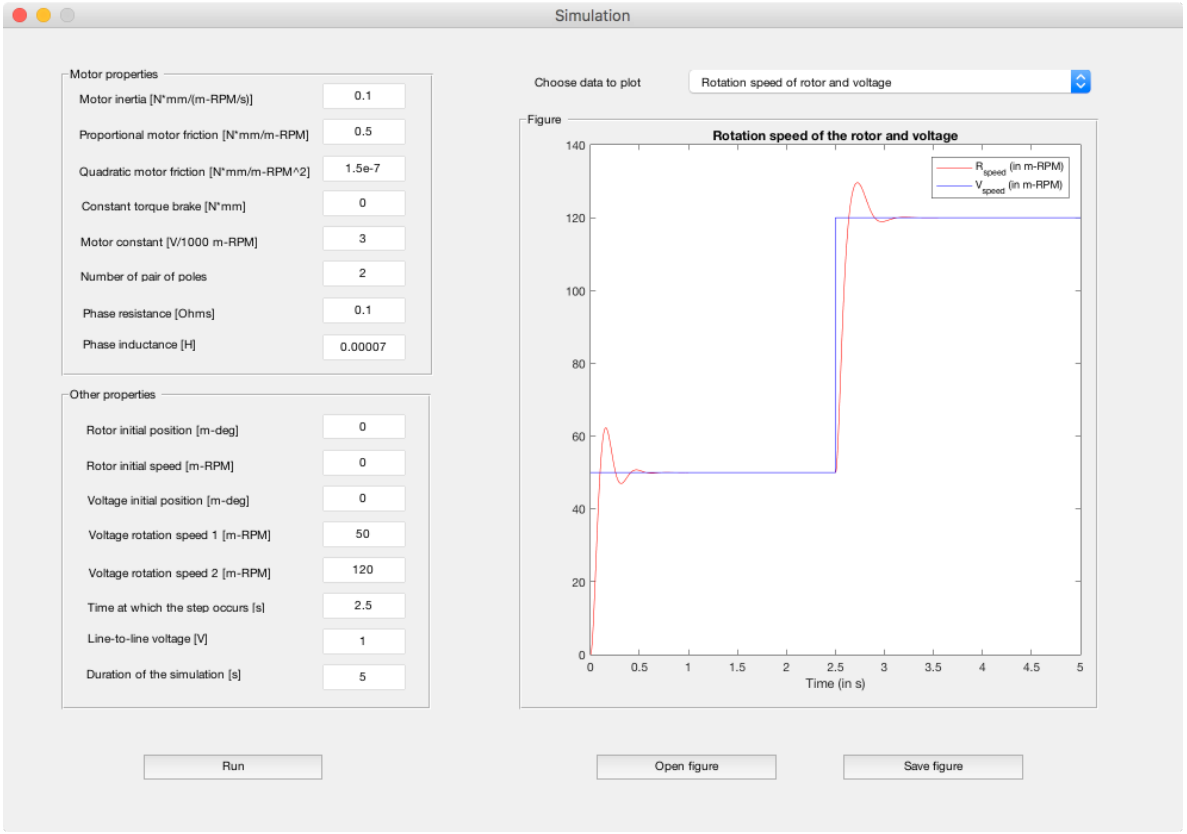

Figure 7.5: GUI allowing the open-loop mechanical characterization, and more specifically the identification of the inertia.

Chapter 8

Electrical parametric analysis

This chapter aims to assess the impact of parameters on the motor's behavior. The electrical parameters are the resistance R, the inductance L and the motor constant K_e.

8.1 Resistance

A general rule is that a resistance induces resistive losses. Therefore, one could think that as the resistance of the system increases, the power loss gets bigger and the efficiency of the motor decreases. However, the reality is a bit more complicated. In closed-loop, one effectively sees a decrease of the efficiency as the resistance increases while in open-loop, the efficiency is increased against all expectations.

Let's first consider the case in closed-loop since it is the most intuitive one. As Table 8.1 illustrates it, when the resistance is increased, the amplitude of the current is decreased. As in closed-loop, the objective is to drive the motor in an efficient way, a zero direct current is desired. Therefore, for both values of the resistance, the direct current stays equal to zero while the quadrature current gets lower for a rise of the resistance. This explains that the driving torque also decreases. Moreover, a lower speed is required in order to obtain a zero IV-angle when the resistance is higher. This leads to a smaller back-emf. As both the rotation speed and the driving torque decrease with an increase of the resistance, the driving power is also reduced. Despite the decrease of the electrical power due to the drop of current, the efficiency of the motor is considerably decreased when the motor resistance is increased.

R (Ω)	0.1	0.2
i_{pk} (A)	2.098	1.639
i_d (A)	0	0
i_q (A)	2.098	1.639
ω (m-RPM)	180.3	140.9
e (V)	0.5408	0.4227
T_{drive} (Nm)	0.09014	0.07045
P_{drive} (W)	1.702	1.039
P_{elec} (W)	2.3621	1.8459
η (%)	72.05	56.29

Table 8.1: Impact of an increase of the resistance on the motor variables in closed-loop with an IV target of 0 degree and a peak voltage of 0.7506 V.

In open-loop, however, the motor behavior following an increase in resistance is completely different. Indeed, when the resistance is increased, the back-emf stays constant and the current decreases. However, in this case, the quadrature current remains the same while the direct current decreases. Therefore, the driving torque as well as the driving power are constant but the electrical power decreases. This leads thus to an increase of the efficiency. Note that if the resistance is increased too much, stalling occurs.

8.2 Inductance

As one sees on Table 8.2, a change in the inductance does not have a huge impact on the motor variables. In fact, when the inductance is increased by one order of magnitude, the efficiency of the motor is decreased by 0.17 %, which is almost negligeable.

8.3 Motor constant

Let's first clearly define the motor efficiency and show its link with the motor constants K_e and K_T.

L (H)	$7 \cdot 10^{-5}$	$7 \cdot 10^{-4}$
i_{pk} (A)	2.098	2.11
i_d (A)	0	-0.1921
i_q (A)	2.098	2.101
ω (m-RPM)	180.3	180.6
e (V)	0.5408	0.5418
T_{drive} (Nm)	0.09013	0.0903
P_{drive} (W)	1.701	1.708
P_{elec} (W)	2.362	2.3756
η (%)	72.02	71.9

Table 8.2: Impact of an increase of the inductance on the motor variables in closed-loop with an IV target of -0.5 degrees and a peak voltage of 0.7506 V.

The motor efficiency η is defined as the ratio between shaft output power and electrical input power:

$$\eta = \frac{P_{out}}{P_{in}} \tag{8.1}$$

where P_{out} is the shaft power output [W],
P_{in} - the electrical power into the motor [W].

The shaft output power is given by:

$$P_{out} = P_{mech} = T\omega \tag{8.2}$$

where T is the driving torque [Nm],
ω - motor angular velocity [rad/s].

And the electrical input power is:

$$P_{in} = P_{elec} = i_a v_a + i_b v_b + i_c v_c = 1.5\, i_{pk} v_{pk}\, cos(IV) \tag{8.3}$$

where i_a, i_b, i_c - phase currents [A],
v_a, v_b, v_c - phase voltages [V],
i_{pk} - peak current [A],
v_{pk} - peak voltage [V],

IV - IV-angle [e-deg].

The power loss can also be computed as:

$$P_{loss} = P_{in} - P_{out} = P_{elec} - P_{mech} \tag{8.4}$$

The loss consists of copper loss caused by the current in the stator armature windings, iron loss caused by flux linkages in the stator and rotor and mechanical loss.

Note also that the motor efficiency η is correlated to the motor constant K_T. Since the driving torque is given by $T_{drive} = K_T \frac{3}{2} i_q$, (8.2) becomes

$$P_{mech} = T_{drive}\,\omega = K_T\,\frac{3}{2}\,i_q\,\omega \tag{8.5}$$

and the motor efficiency can be written as

$$\eta = \frac{K_T\,\frac{3}{2}\,i_q\,\omega}{\frac{3}{2}\,i_{pk} v_{pk}\,cos(IV)} = K_T\,\frac{i_q\,\omega}{i_{pk} v_{pk}\,cos(IV)} \tag{8.6}$$

Let's recall that if the motor constants K_e and K_T are expressed in the SI units, i.e. K_e in [V/(rad/s)] and K_T in [Nm/A], then

$$K_e = K_T \tag{8.7}$$

As (8.6) suggests it, the motor efficiency increases as the motor constant increases, and vice versa (cf. Table 8.3). However, for a given voltage, when $K_T = K_e$ is too high, it will not be possible to achieve the desired speed. The reason behind this is that the voltage will not be sufficient since a great back-emf will be generated. Contrariwise, if $K_T = K_e$ is too low, the current needed to achieve the desired torque will be higher than necessary.

K_e (V/1000 m-RPM)	2	3	4
η (%)	53.34	72.05	82.08

Table 8.3: Impact of a change of the motor constant on the motor efficiency in closed-loop.

Chapter 9

Mechanical parametric analysis

The mechanical parameters are the inertia J, the friction and the load of the motor system $Fr2_m$, Fr_m and T_0. In addition, the influence of some other properties such as the sweep frequency, the cogging torque or the torque shock is studied hereafter.

9.1 Inertia

The inertia of the motor does not have any influence on the steady-state values of the motor variables in closed-loop. It only changes the dynamic of the motor during start-up time. Indeed, as illustrated on Figure 9.1, more oscillations appear as the inertia increases. It results in more noise, and also leads to oscillations in the current which could eventually damage the motor at some point.

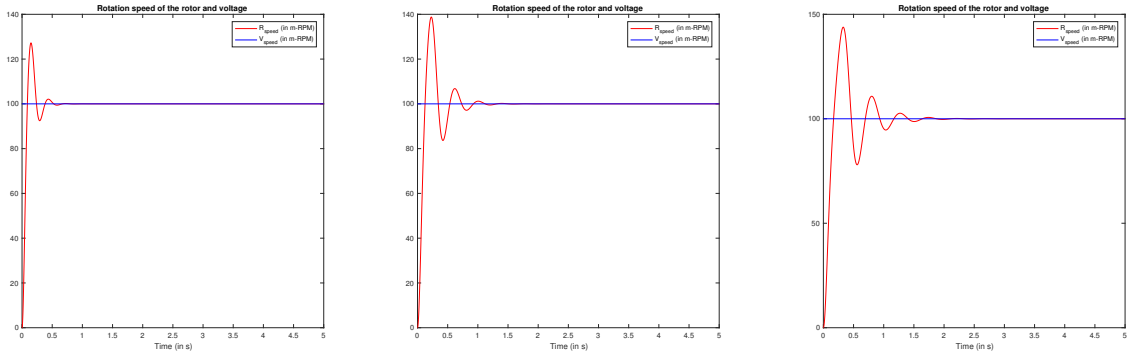

(a) J = 0.1 Nmm/(m-RPM/s) (b) J = 0.2 Nmm/(m-RPM/s) (c) J = 0.3 Nmm/(m-RPM/s)

Figure 9.1: Impact of the inertia J on the dynamic of the motor in open-loop. Graphs of the rotation speed for increasing values of J.

9.2 Friction and load of the motor

Generally speaking, the system reaches equilibrium at some point where the electromagnetic torque (T_{drive}) matches the motor's mechanical load (T_{mech}). If the mechanical load is increased, current will increase to match that torque as speed slows down, making more Ri drop voltage available (since the back-emf voltage decreases in this case). Table 9.1 provides a numerical example. Futhermore, this shows that the motor efficiency decreases as the load or the friction increases. If the external load becomes too high, the controllability of the motor will be lost. Indeed, the available voltage will not be enough to provide the required current and torque.

T_{mech} (Nm)	0.09014	0.1135
ω (m-RPM)	180.3	162.1
e (V)	0.5407	0.4864
i_{pk} (A)	2.098	2.641
i_q (A)	2.098	2.641
T_{drive} (Nm)	0.09014	0.1135
P_{drive} (W)	1.702	1.927
P_{elec} (W)	2.3621	2.9735
η (%)	72.05	64.81

Table 9.1: Impact of an increase of the friction/load on the motor variables in closed-loop with an IV target of 0 degree and a peak voltage of 0.7506 V.

9.3 Other parameters

Sweep properties As mentioned in subsection 5.2.7, starting the motor with a sweep in frequency allows to reduce oscillations, and reach higher speeds in open-loop.

Cogging torque Cogging torque leads to oscillations in all motor variables without any exception, which results in noise. Therefore, it is an undesirable effect which needs to be compensated in order to reduce the ambient noise.

However, it seems that the cogging torque is not really critical for the control of the motor. Even when the amplitude of the cogging torque is of the same order as the mechanical torque, the rotor is still able to follow the stator rotating field.

Torque shock In the same way as the cogging torque, a torque shock induces an oscillation in all motor variables. As long as the amplitude is not too high, it does not lead to controllability problems. However, when the amplitude of the torque shock becomes very high compared to the mechanical torque, one sees on Figure 9.2 that there is a short lost of synchronization (about half a second), and then the rotor starts rotating normally again.

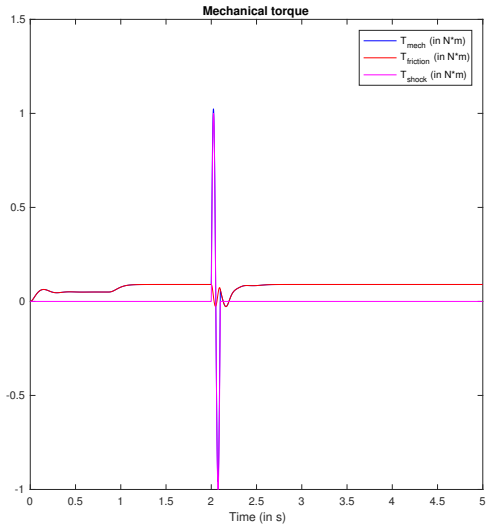

(a) Mechanical torque.

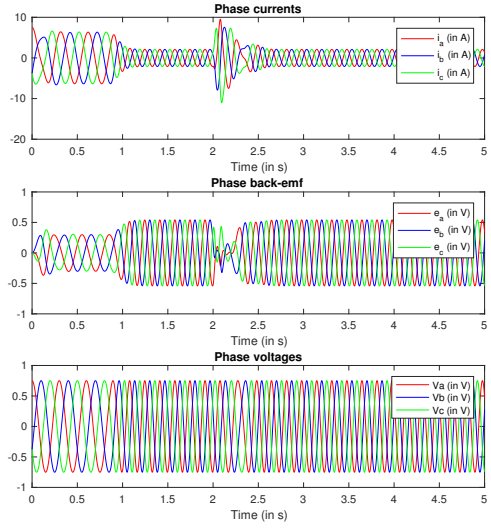

(b) Current, back-emf and voltage in a fixed reference frame.

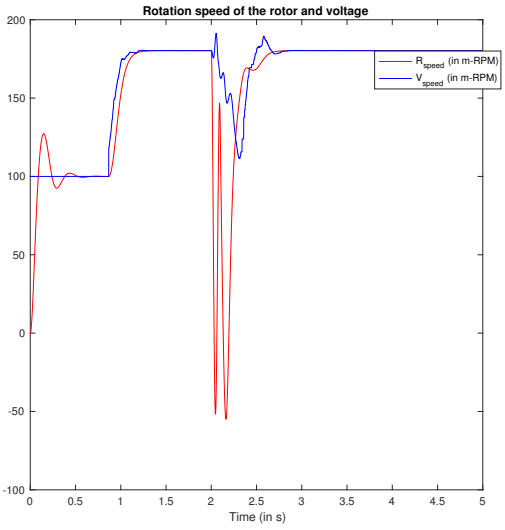

(c) Rotation speed.

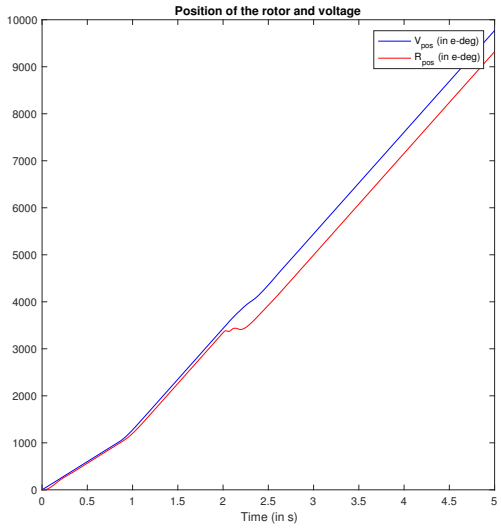

(d) Position.

Figure 9.2: Impact of a torque shock on the controllability of the motor (the torque shock is a sine cycle of 1Nm of amplitude with a period of 0.1s).

Chapter 10

Conclusion

In this thesis, a Matlab model of a three-phase BLDC motor was developed. The aim was to make a model that would be simple, accurate, and easy to modify. Several options were added in order to make it more realistic. For easy handling, an intuitive GUI was implemented to run the simulations. It makes it very simple to change the parameters of a motor, to choose whether inductance, cogging torque or torque shock need to be modelled, to select a frequency sweep, and even to pick a closed-loop scenario. Moreover, this window allows you to plot the results of the simulation, which can be chosen among a broad choice of graphs. A sensorless control strategy based on motor current and voltage measurements (self-sensing solution) was applied, leading to high efficiency, while sinusoidal phase currents contribute to smooth torque, and hence, low noise. As datasheets are not always available for all motors, this document also provides methods to identify the parameters that are necessary to the model. Finally, a parametric analysis was performed in order to better understand and highlight some behaviors of the motor following parameters variations.

This model will be used as a tool which can be useful to Melexis employees. As an example, an application engineer from the actuator business unit came to me during my internship in order to perform a simulation. The purpose was to pinpoint the noise source in his control algorithm. The results of the simulation showed that the impact of a time shift between current and voltage measurements on PID-regulation is the appearance of a saw-tooth behavior. This saw-tooth behavior which was observed could be the source of the noise. Therefore, based on the results, they implemented an additional compensation in the software to reduce noise.

This thesis (and of course the internship) was a valuable experience as a student. I learned how to work independently on a big project, in a real working environment. I had the opportunity to discover a lot about the company by talking to several employees from different departments. In short, working during more than 4 months within a well-known international company like Melexis has definitely been very rewarding. Furthermore, I was warmly welcomed within Melexis, and directly integrated into the team.

10.1 Future work

Despite that this model gives intuitive results that seem correct at first glance, it is essential to use real measurements to fit the model. A comparaison of the simulation results with real measurements must be performed. Furthermore, the range of validity of the model should be derived. The model should be tested with the parameters of a small BLDC cooling fan ($\sim 10W$) as well as with those of a big BLDC hvac blower ($\sim 250W$).

Other control methods could also be tested on the model. A fast-loop with V-angle tracking based on IV-error (BLDC commutation loop) was already implemented, but the implementation of a slow-loop with V-amplitude modification based on speed-error or torque-error ("DC motor loop") would be the logical next step. Additionally, a study of the PID coefficients versus regulation stability could be performed.

Appendices

Appendix A

Strategy of Melexis

This is a non-technical chapter which aims to present Melexis N.V. and the strategic aspects of the company. These strategic aspects include marketing strategy, human ressources strategy, financial strategy and R&D strategy.

A.1 About Melexis

Melexis is one of the five world leaders in automotive semiconductor sensors, as well as a leading player in integrated circuits for motor driving, car networking and wireless communication [8]. Indeed, Melexis is an automotive integrated circuit manufacturer that designs, develops, tests and markets integrated circuits for automotive electronics systems.

Wide range of product Melexis develops both ASICs (application specific integrated circuits) and ASSPs (application specific standard products). The product portfolio of Melexis includes temperature sensors, pressure sensors, current sensors, optical sensors, position and speed sensors, embedded motor drivers, LED drivers, fan drivers, LIN (local interconnect network) system chips, wireless sensors and others.

Over the world The company operates through its subsidiaries and branch offices in Belgium, Bulgaria, China, France, Germany, Hong Kong, Japan, Philippines, Switzerland, Ukraine, USA and Malaysia. Melexis is rooted in Ieper, Belgium.

Automotive industry and beyond Melexis is not only active in the automotive area but also in the smart appliances, home automation, industrial and medical sectors.

Customer driven innovation Melexis has a customer-centered approach that has been fundamental to its success.

Future trends From magnetic sensor and sensor interfaces, to wireless and actuators, Melexis is constantly innovating to create more sustainable and more reliable vehicles. Looking forward in the automotive industry there is excitement around the potential for autonomous cars, and this trend is helping to shape the future of Melexis.

Future growth Since the birth of the company in Belgium in 1988, Melexis has grown to over 1,100 employees in 14 countries.

Sales summary In 2016, Melexis surpassed the 450 million EUR sales threshold, nearly doubling sales compared to 2011. Sales for the first quarter of 2017 were 123.6 million EUR, an increase of 13% compared to the same quarter of the previous year and an increase of 3% compared to the previous quarter [11].

A.1.1 Corporate governance

Board of Directors The main responsibilities of the Board of Directors relate to giving strategic direction to the company and the supervision of the state of affairs [10]. The Board of Directors comprises at least five Directors. The Board of Directors delegates the daily management of the company to the Chief Executive Officer who is assisted by the Executive Management.

Executive management The Executive Management is composed of the CEO, the CFO, 3 Business Unit Managers and 5 Global Managers. The Executive Management has the operational accountability for leading the Company in accordance with the global strategy, vision, mission and values, and with the planning and budgets approved by the Board of Directors.

The Business Unit Managers are responsible for developing the business across the regions and focus on their customers' interests and future business development in the four business units Sensors, Actuators, Opto and Wireless.

The Global Managers are responsible for functional excellence and compliance in Development, Operations/IT, Quality, Sales and Marcom, and Human Resources.

A.2 Strategy

The key elements of the company's strategy are [9]:

a) Simply the best innovation made safe at launch, on time Melexis' growth is certainly due to its customer focus and its consistent strategic vision. Creating innovative products and bringing them into production in a timely and reliable way is essential to the success of Melexis and that of their customers. The company will continue to build on its knowledge and experience, expanding its scope to include new applications, new sectors and new markets.

b) Continuing opportunities for growth in the automotive sector Management believes that the market for automotive semiconductors offers high growth opportunities. Despite modest growth in car sales, the amount of electronics built into vehicles is steadily increasing year after year. Consequently, Melexis core business will focus on advanced integrated semiconductor devices for automotive applications. This will allow the company to benefit from its experience, engineering excellence and competitive advantage in the design, development and testing of such devices. These electronics allow car manufacturers to differentiate their cars from the competition by adding electronic comfort features, or offering higher standards of safety or economy. Melexis has also observed interesting growth in new markets and sectors, including consumer electronics, wireless and industrial applications and personal healthcare.

c) Focus on ASSPs and ASICs ASICs and ASSPs are broad and generally accepted building blocks for all kinds of applications. ASIC customers have good reason to trust Melexis for their mixed-signal ICs and sensor parts. Melexis puts high priority on offering more than just a finished and tested component based on the customer's block diagram: the responsible teams actively think of ways to design, develop and deliver customized ASIC solutions. Innovative, progressive solutions at the schematic level and throughout the lifecycle of the program make the difference.

d) Partner of choice Melexis focuses on a product's complete lifecycle. That is why they maintain close working relationships with their customers and their suppliers. The company seeks for strong continuity in these collaborative activities, especially in the field of development, engineering and technical support. This allows Melexis to go beyond developing a good product. It offers crucial insight and the big-picture perspective needed to develop applications that anticipate future plans and needs, new trends and emerging markets.

e) Leading the way in sensor and actuator solutions Melexis has a well-matched team of experienced engineers. Their expertise in product definition, design and testing of integrated analogue-digital sensor and actuator solutions and sensor chips has given Melexis a leading position. To maintain and strengthen this position, Melexis is making substantial investments in R&D.

f) First for quality and environmental awareness Recognized standards are of crucial importance in the automotive industry, one of the most challenging sectors in the world, and are therefore also essential to suppliers like Melexis. Vehicle manufacturers must be able to trust suppliers to have their processes under control, understand their customers' needs and continue to innovate. The ISO/ TS 16949 quality management system certificate demonstrates that Melexis meets all these criteria. Melexis makes consistent efforts for improvement to all processes and at all sites.

A.2.1 R&D strategy

Research and Development expenses amounted to EUR 63 million in 2016, representing 14% of total revenue, versus EUR 56 million in 2015 [9]. The company invests significantly in its research and development department. R&D is the principal activity of many sites of the company including Ukrainian, German or Belgian sites.

A.2.2 HR strategy

Employees of the company are mostly highly skilled. Melexis employs a large number of engineers. They are separated according to their skills in different departments during the recruitment. However, the company offers possibilities to switch to another department in order to find the right place for each employee. Indeed, Melexis aims to

put the right people at the right place. This approach ensures intrinsic motivation and job satisfaction. Moreover, according to workers in Tessenderlo, the company is very flexible. Melexis allows employees to relocate, to adapt their working schedule, etc.

In conclusion, the strategy of Melexis is focused on innovation in both its new and established product ranges, allowing them to take advantage of beneficial market developments in sectors including automotive, industry, medical, and home and building automation. With their expertise in product definition, design, and testing for integrated analog or digital semiconductor solutions and sensor chips, the company is sure to maintain its commanding market position. The successful strategy of Melexis allows the company to grow year after year. Figure A.1 shows the evolution of the company revenue from 2012 to 2016. In order to support this growth, Melexis will continue to devote resources to research & development, sales & marketing, and automation. The planned investments in buildings, infrastructure and equipment for 2017 will amount to a total of approximately EUR 40 million [9].

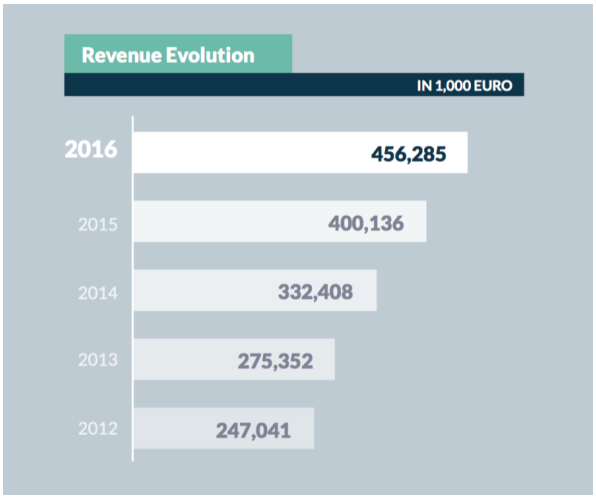

Figure A.1: Evolution of Melexis' revenue from 2012 to 2016. Source [9].

Appendix B

Parameter data set

This chapter contains the value of the parameters used in the simulations presented and analyzed in this document.

Simulation 1

Motor inertia (Nmm/(m-RPM/s))	0.1
Proportional motor friction (Nmm/m-RPM)	0.5
Quadratic motor friction (Nmm/m-RPM^2)	1.5e-7
Constant torque brake (Nmm)	0
Motor constant (V/1000 m-RPM)	3
Number of pole pairs	2
Phase resistance (Ohms)	0.1
Phase inductance (H)	*No*
Rotor initial position (m-deg)	0
Rotor initial speed (m-RPM)	0
Voltage initial position (m-deg)	0
Frequency sweep	*No*
Voltage rotation speed (m-RPM)	100
Line-to-line voltage (V)	1.3
Cogging torque	*No*
Torque shock	*No*
Closed-loop	*No*

Table B.1: Value of the parameters used for simulation 1.

Simulation 2

Motor inertia (Nmm/(m-RPM/s))	0.1
Proportional motor friction (Nmm/m-RPM)	0.5
Quadratic motor friction (Nmm/m-RPM^2)	1.5e-7
Constant torque brake (Nmm)	0
Motor constant (V/1000 m-RPM)	3
Number of pole pairs	2
Phase resistance (Ohms)	0.1
Phase inductance (H)	*No*
Rotor initial position (m-deg)	0
Rotor initial speed (m-RPM)	0
Voltage initial position (m-deg)	0
Frequency sweep	*Yes*
Voltage start rotation speed (m-RPM)	0
Voltage end rotation speed (m-RPM)	170
Voltage acceleration (m-RPM/s)	200
Line-to-line voltage (V)	1.3
Cogging torque	*No*
Torque shock	*No*
Closed-loop	*No*

Table B.2: Value of the parameters used for simulation 2.

Simulation 3

Motor inertia (Nmm/(m-RPM/s))	0.1
Proportional motor friction (Nmm/m-RPM)	0.5
Quadratic motor friction (Nmm/m-RPM^2)	1.5e-7
Constant torque brake (Nmm)	0
Motor constant (V/1000 m-RPM)	3
Number of pole pairs	2
Phase resistance (Ohms)	0.1
Phase inductance (H)	*No*
Rotor initial position (m-deg)	0
Rotor initial speed (m-RPM)	0
Voltage initial position (m-deg)	0
Frequency sweep	*No*
Voltage rotation speed (m-RPM)	100
Line-to-line voltage (V)	1.3
Cogging torque	*Yes*
Torque shock	*No*
Closed-loop	*No*

Table B.3: Value of the parameters used for simulation 3.

T_{cog} (Nmm)	θ_m (m-degrees)		T_{cog} (cont.)	θ_m (cont.)		T_{cog} (cont.)	θ_m (cont.)
0	0		-6,5	125		7	250
-7,5	5		2,5	130		0	255
5	10		0	135		-6	260
-2,5	15		-8	140		6	265
-9	20		3	145		0	270
7,5	25		0	150		-7	275
0,5	30		-7,5	155		5	280
-6	35		5	160		-2,5	285
5	40		0	165		-8	290
0	45		-6,5	170		8	295
-8,5	50		4	175		1	300
2	55		0	180		-5,5	305
0,5	60		-7,5	185		5,5	310
-7,5	65		4,5	190		-4	315
5	70		-3	195		-7,5	320
0	75		-9	200		5	325
-6	80		7,5	205		-2	330
5	85		1	210		-7,5	335
0	90		-6	215		7	340
-7,5	95		6	220		-0,5	345
4	100		-1	225		-6,5	350
0	105		-7,5	230		6	355
-8,5	110		5,5	235		0	360
7,5	115		-1	240			
1	120		-6,5	245			

Table B.4: Amplitude of the cogging torque T_{cog} as a function of the mechanical rotor position θ_m.

Simulation 4

Motor inertia (Nmm/(m-RPM/s))	0.1
Proportional motor friction (Nmm/m-RPM)	0.5
Quadratic motor friction (Nmm/m-RPM^2)	1.5e-7
Constant torque brake (Nmm)	0
Motor constant (V/1000 m-RPM)	3
Number of pole pairs	2
Phase resistance (Ohms)	0.1
Phase inductance (H)	*No*
Rotor initial position (m-deg)	0
Rotor initial speed (m-RPM)	0
Voltage initial position (m-deg)	0
Frequency sweep	*No*
Voltage rotation speed (m-RPM)	100
Line-to-line voltage (V)	1.3
Cogging torque	*No*
Torque shock	*Yes*
Time at which it occurs (s)	0.6
Period of the sine cycle (s)	0.2
Amplitude of the sine cycle (Nm)	0.03
Closed-loop	*No*

Table B.5: Value of the parameters used for simulation 4.

Bibliography

[1] S. Baldursson. "BLDC Motor Modelling and Control - A Matlab®/Simulink® Implementation". MA thesis. Chalmers Tekniska Högskola, 2005.

[2] Viktor Bobek. *PMSM Electrical Parameters Measurement*. 2013.

[3] Tech Briefs. *Reasons for Turning to Slotless DC Motor Technology*. 2015. URL: http://www.techbriefs.com/component/content/article/22932.

[4] W. Brown. "Brushless DC Motor Control Made Easy". In: *Microchip Technology Inc.* (2002).

[5] J. C. Gamazo-Real, E. Vazquez-Sanchez, and J. Gomez-Gil. "Position and Speed Control of Brushless DC Motors Using Sensorless Techniques and Application Trends". In: *sensors* (2010), pp. 6901–6947.

[6] A. Hartman and W. Lorimer. *Cogging torque control in brushless DC motors*. 2000.

[7] S. Lee, T. Lemley, and G. Keohane. *A comparison study of the commutation methods for the three-phase permanent magnet brushless DC motor*.

[8] Melexis. *About us*. URL: https://www.melexis.com/en/about-us (visited on 05/11/2017).

[9] Melexis. *Annual Report 2016*. Mar. 2017.

[10] Melexis. *Investors - Corporate Governance*. URL: https://www.melexis.com/en/investors/corporate-governance/board-of-directors (visited on 05/11/2017).

[11] Melexis. *News - Melexis Q1 2017 results*. URL: https://www.melexis.com/en/news/2017/financial/melexis-q1-2017-results (visited on 05/11/2017).

[12] Microsemi. "Park, Inverse Park and Clarke, Inverse Clarke Transformations MSS Software Implementations User Guide". In: (), p. 5.

[13] B. Tibor, V. Fedak, and F. Durovsky. "Modeling and Simulation of the BLDC Motor in MATLAB GUI". In: *IEEE* (2011), pp. 1403–1407.

[14] Wikipedia. *PID controller*. 2017. URL: `https://en.wikipedia.org/wiki/PID_controller`.

[15] digitalPimple Youtube. *Brushless DC Motors & Control - How it Works*. 2012. URL: `https://www.youtube.com/watch?v=ZAY5JInyHXY`.

[16] Z. Q. Zhu and D. Howe. "Influence of Design Parameters on Cogging Torque in Permanent Magnet Machines". In: *IEEE Transactions on Energy Conversion* 15.4 (Dec. 2000), pp. 407–412.